BEILSTEIN JOURNAL OF ORGANIC CHEMISTRY

Recent advances in chiral aluminum asymmetric catalysis: ligand design, coordination modulation, and structure–activity relationships

Tianzhe Wen, Xiaoli Ma*, Ziyuan Pang, Xiaobo Yang and Zhi Yang*

Review

Open Access

Address:
School of Chemistry and Chemical Engineering, Beijing Institute of Technology, Beijing 100081 P. R. China

Email:
Xiaoli Ma* - maxiaoli@bit.edu.cn;
Zhi Yang* - zhiyang@bit.edu.cn

* Corresponding author

Keywords:
asymmetric catalysis; chiral aluminum catalysts; coordination modulation; enantioselectivity; ligand design

Beilstein J. Org. Chem. **2026,** *22,* 1605–1627.
https://doi.org/10.3762/bjoc.22.130

Received: 23 March 2026
Accepted: 14 October 2026
Published: 09 November 2026

Associate Editor: S. Bräse

© 2026 Wen et al.; licensee Beilstein-Institut.
License and terms: see end of document.

Abstract

The development of sustainable strategies for asymmetric catalysis remains a central goal in modern synthetic chemistry. Chiral aluminum catalysts, derived from earth-abundant and low-toxicity main-group elements, are emerging as powerful alternatives to precious transition-metal systems. This review systematically surveys two decades of progress in chiral aluminum asymmetric catalysis, with a central focus on the fundamental correlation between rational ligand design, coordination environment tuning at aluminum centers, and the resulting structure–activity/selectivity relationships. We highlight how modular ligand engineering including 1,1'-binaphthyl-2,2'-diol (BINOL), salen, and N-heterocyclic scaffolds enables precise control over aluminum's coordination geometry, Lewis acidity, and chiral microenvironment, delivering high enantio- and regiocontrol across diverse reactions from cycloadditions and asymmetric reductions to C–H functionalization and stereoselective polymerization. Beyond their cost and environmental advantages, these systems showcase unique stereocontrol mechanisms arising from metal-centered chirality and cooperative catalysis. Challenges remain in expanding substrate scope and improving recyclability, but continued innovation promises to establish aluminum catalysis as a frontier platform for the sustainable synthesis of pharmaceuticals, fine chemicals, and functional materials.

Introduction

Chirality is a fundamental concept in chemistry, describing the geometric properties of molecules that are not superimposable on their mirror images. This structural feature is critically important because enantiomers often display markedly different chemical reactivities, biological activities, and physical properties [1-5]. As a result, the selective synthesis of optically active compounds has become a central objective in contemporary chemical research, particularly in the fields of pharmaceuticals, agrochemicals, fine chemicals, and functional materials.

Among the various strategies developed to access chiral molecules, asymmetric catalysis stands out as one of the most efficient and versatile approaches. By enabling the catalytic generation of chirality from achiral or prochiral substrates, asymmetric catalysis offers significant advantages in terms of atom economy, reaction efficiency, and functional group tolerance. Over the past several decades, remarkable progress has been achieved through the development of chiral transition-metal catalysts, especially those based on rhodium [6-13], ruthenium [14-20], and iridium [10,12,21-23]. These systems benefit from flexible coordination geometries, tunable electronic structures, and the ability to access multiple oxidation states, which together facilitate precise stereochemical control in a wide range of transformations. Despite their success, transition-metal-based asymmetric catalysts are associated with several inherent limitations. The high cost and limited natural abundance of many transition metals, combined with concerns regarding toxicity, metal residues, and environmental impact, pose challenges for large-scale and industrial applications [24]. These considerations have motivated increasing interest in catalytic systems based on main-group elements as complementary alternatives for asymmetric synthesis.

In this context, aluminum has emerged as a particularly attractive main-group metal for asymmetric catalysis [25]. Aluminum is the most abundant metal in the Earth's crust, is inexpensive, and exhibits low toxicity, making it well suited for sustainable catalytic applications [26,27]. From a coordination chemistry perspective, aluminum displays strong Lewis acidity and can adopt a variety of coordination numbers, typically ranging from four to six, as well as hypercoordinated geometries [28]. This structural flexibility endows aluminum centers with excellent modifiability, allowing the coordination modulation of aluminum through rational ligand design to construct well-defined chiral microenvironments, and further establish clear structure–activity relationships between the catalyst structure and catalytic performance [29,30].

Over the past two decades, substantial advances have been made in the design of chiral aluminum catalysts through the development of well-defined ligand frameworks. Among these, BINOL-derived ligands have played a central role due to their rigid axial chirality, strong chelating ability, and capacity to stabilize aluminum centers in both tetra- and hexacoordinate environments [31-33]. Chiral salen ligands, with their tetradentate coordination modes and modular steric and electronic tunability, have enabled precise control over aluminum coordination geometry and have been widely applied in asymmetric carbon–carbon-bond formation and polymerization reactions [34,35]. In parallel, nitrogen-containing heterocyclic ligands, including oxazolines, pyrrolidines, and scorpionate-type frameworks, have expanded the structural diversity of chiral aluminum complexes and provided new opportunities for fine-tuning catalyst reactivity and stereoselectivity [36-38].

This review summarizes the progress achieved in chiral aluminum catalysis over the past two decades from an inorganic and coordination chemistry perspective. The discussion is organized according to major ligand classes, including BINOL-based aluminum catalysts, chiral salen aluminum complexes, nitrogen heterocycle-supported aluminum systems, and other emerging ligand architectures. Emphasis is placed on the coordination environment of the aluminum center, ligand design principles, and their influence on catalytic performance and stereochemical outcomes. By highlighting representative examples and key mechanistic concepts, this review aims to provide a comprehensive overview of chiral aluminum catalysis and to serve as a reference for the rational design of next-generation main-group asymmetric catalysts.

Review

BINOL-based chiral aluminum catalysts

Since the 1990s, BINOL has been widely employed as a chiral ligand in asymmetric catalysis, where it has demonstrated distinctive stereocontrol capabilities. Early studies primarily focused on BINOL transition-metal complexes [39-41], while the catalytic potential of aluminum as a main-group element was gradually revealed in the early twenty-first century. Among the various ligand platforms developed for asymmetric aluminum catalysis, BINOL-derived systems have become the most extensively investigated because their rigid, yet tunable framework enables effective modulation of the aluminum coordination environment and catalytic performance [42].

Coordination geometry effects on catalytic performance

A distinctive characteristic of BINOL-supported aluminum catalysts is the ability of the aluminum center to adopt diverse coordination geometries. Depending on the ligand architecture and ancillary donor groups, tetrahedral, pentacoordinate, hexacoordinate, and even hypercoordinated aluminum species can be generated. These structural variations significantly influence the catalytic reactivity and stereoselectivity [33].

Early efforts focused on the construction of hypercoordinated aluminum complexes. Simonsen et al. [43] reported a series of hypercoordinated aluminum catalysts. By introducing multidentate ligands, the Lewis acidity of the aluminum center was enhanced, and the use of bulky ligands **1a**–**d** restricted the approach of substrates. Notably, ligands **1b** and **1c** achieved hypercoordination through the incorporation of ether oxygen atoms, thereby increasing the electron density at the aluminum

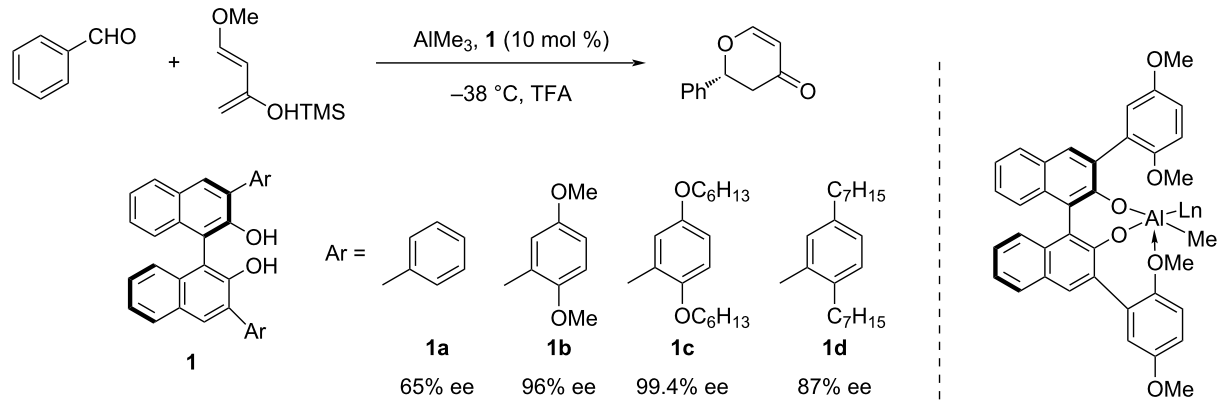
center, stabilizing the reaction intermediates, and markedly enhancing enantioselectivity. In the hetero-Diels–Alder reaction between benzaldehyde and Danishefsky's diene, the highest enantioselectivity was achieved with ligand **1c**, affording an optimal ee value of 99.4% (Scheme 1). Mechanistically, the additional donor atoms not only stabilized the aluminum center but also restricted conformational flexibility, thereby creating a more defined chiral pocket for substrate activation.

The asymmetric Meerwein–Ponndorf–Verley (MPV) reduction represents a classical Lewis acid-mediated transformation in aluminum catalysis. Nguyen et al. [44] applied the active species [(BINOL)Al(OiPr)] **2** and **3**, generated in a 1:1 ratio from $AlMe_3$ with either (*R*)-BINOL or (*S*)-BINOL, to the asymmetric MPV reduction of prochiral ketones. The active species was proposed to be a monomeric, tetracoordinate aluminum complex. Under these conditions, electron-deficient aryl ketones exhibited excellent reactivity and enantioselectivity. For instance, α-bromoacetophenone was reduced to 99% yield with 83% ee, whereas unsubstituted acetophenone delivered only 28% ee, indicating a strong substrate-dependent stereochemical outcome (Scheme 2).

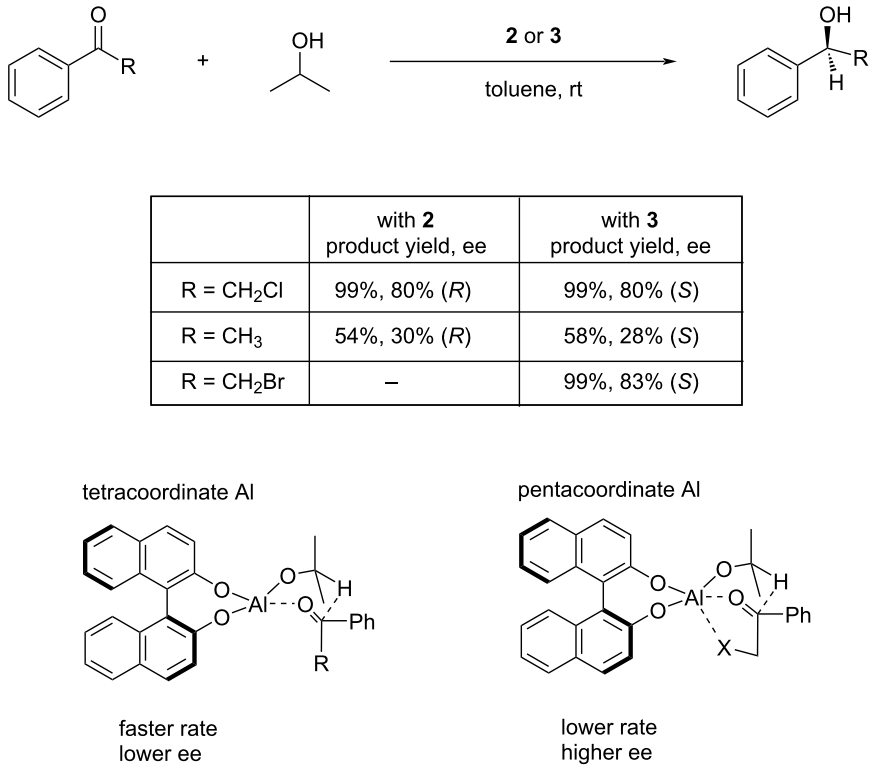
A subsequent mechanistic study in 2007 provided further insight into the nature of the active species and its coordination environment [45]. Spectroscopic and mass spectrometric analyses suggested that, in solution, the catalytic system may involve solvent-coordinated pentacoordinate aluminum species, indicating a more complex coordination landscape than the originally proposed tetracoordinate model. Substrates bearing additional coordinating groups can form a rigid two-point binding mode through simultaneous coordination of the carbonyl oxygen and the α-substituent, significantly restricting transition-state flexibility and enabling high enantioselectivity. In contrast, simple ketones such as acetophenone can only engage in one-point binding, leading to a more flexible transition state and much lower enantioselectivity (Scheme 2). Overall, these studies demonstrate that the coordination geometry of the aluminum center governs both substrate binding mode and transition-state rigidity, making it a key factor for controlling catalytic efficiency and enantioselectivity in BINOL-based aluminum catalysis.

With an improved mechanistic understanding of aluminum-catalyzed processes, researchers systematically optimized the BINOL ligand framework to broaden the reaction scope. Harada et al. [46] reported a dinuclear aluminum catalyst derived from DPP-H_8-BINOL ligand **4** and $AlMe_3$, which promoted the asymmetric vinylation of aldehydes to yield allylic alcohols with up to 89% ee. The reaction proceeded under mild conditions with minimal side reactions (Scheme 3). This study overcame the limitations of conventional titanium-based catalytic systems and, for the first time, demonstrated that aluminum catalysts can directly promote the asymmetric addition of vinylaluminum reagents to aldehydes, thereby reducing both cost and operational complexity.

A recent breakthrough further expanded this concept through the isolation of a well-defined hexacoordinate BINOL aluminum alkoxide complex. Li et al. [47], building on Rueping's work, employed the (*R*)-CF_3-BINOL ligand in the asymmetric hydroboration of heteroaryl ketones using HBpin as the hydroboration reagent to afford chiral alcohols. Experimental results showed that when the in situ-generated catalyst **5** was employed, substrates bearing electron-donating groups achieved enantioselectivities of 97 to 98% ee, whereas those with electron-withdrawing groups reached 87% ee. When the isolated hexacoordinate aluminum alkoxide complex was used as the catalyst, enantioselectivity increased significantly to 98 to

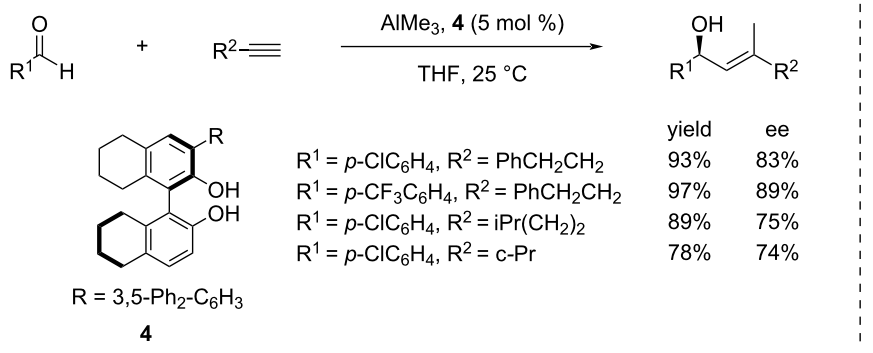


Scheme 1: Hetero-Diels–Alder reaction of benzaldehyde with Danishefsky dienes catalyzed by organoaluminum compounds containing ligands **1**.



	with **2** product yield, ee	with **3** product yield, ee
R = CH_2Cl	99%, 80% (*R*)	99%, 80% (*S*)
R = CH_3	54%, 30% (*R*)	58%, 28% (*S*)
R = CH_2Br	–	99%, 83% (*S*)

Scheme 2: Asymmetric reduction of aromatic ketones catalyzed by organoaluminum compounds **2** and **3**.

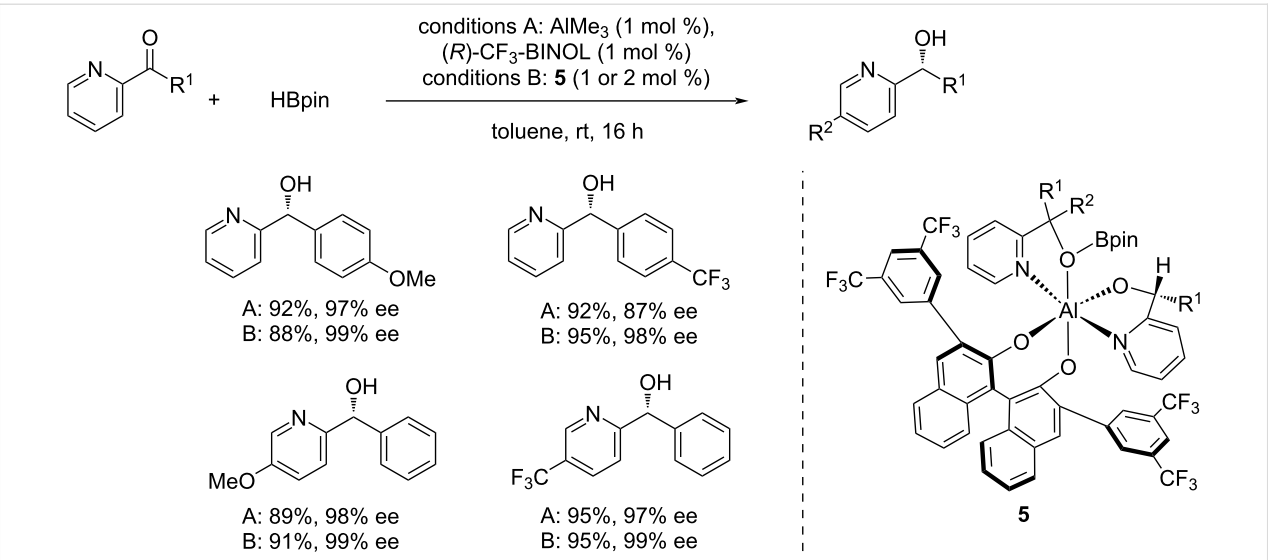


	yield	ee
R^1 = *p*-ClC_6H_4, R^2 = $PhCH_2CH_2$	93%	83%
R^1 = *p*-$CF_3C_6H_4$, R^2 = $PhCH_2CH_2$	97%	89%
R^1 = *p*-ClC_6H_4, R^2 = $iPr(CH_2)_2$	89%	75%
R^1 = *p*-ClC_6H_4, R^2 = c-Pr	78%	74%

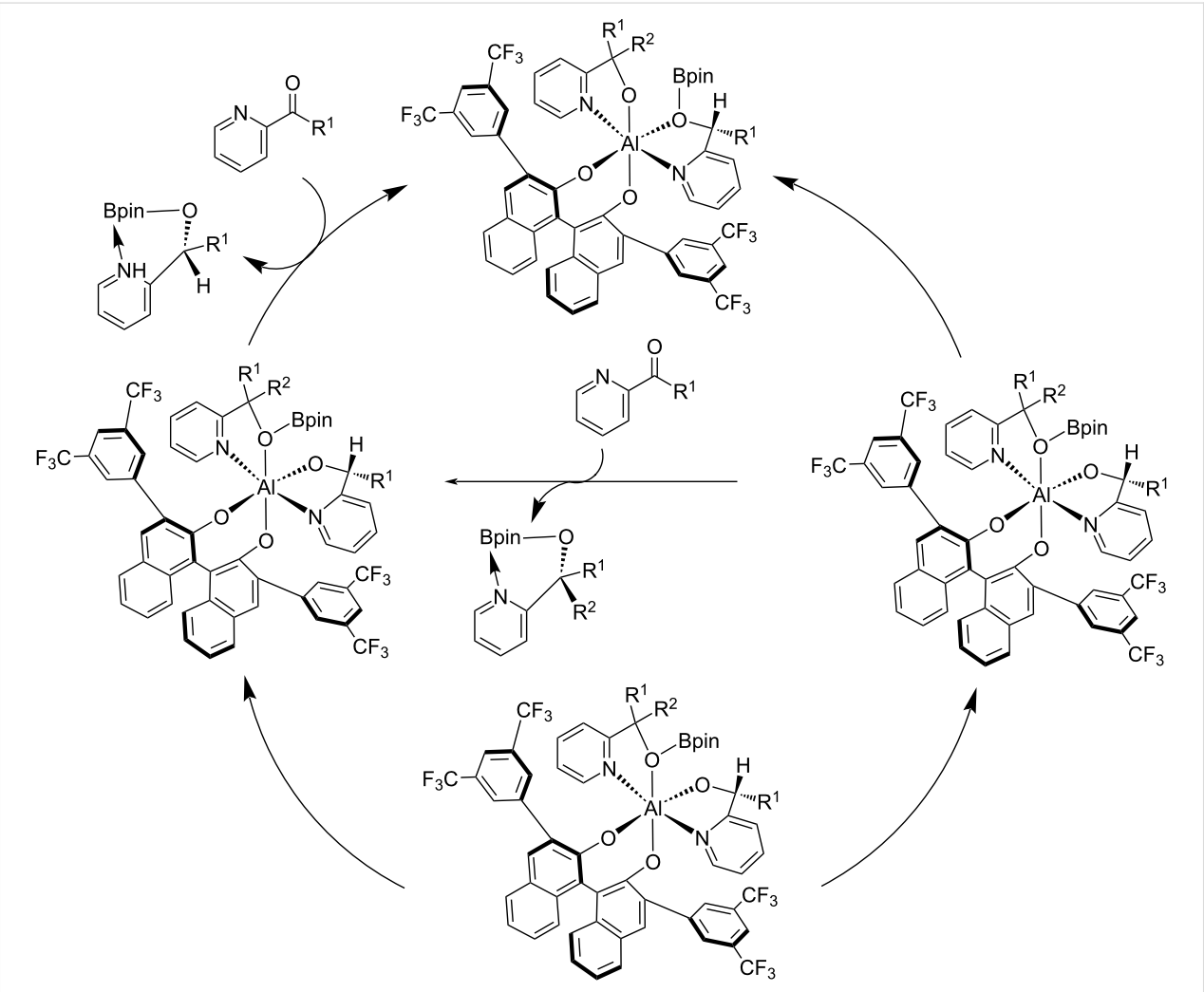
Scheme 3: Asymmetric vinylation of aldehydes catalyzed by organoaluminum compounds containing ligand **4**.

99% ee (Scheme 4). The highest stereoselectivity was obtained under conditions employing the isolated catalyst, with excellent conversion and minimal sensitivity to electronic effects. The key conclusion revealed a novel catalytic mechanism involving an octahedral chiral aluminum center, in which stereochemical control is governed by BINOL-induced chirality at the aluminum center. This finding overcomes the limitations of traditional hydroalumination mechanisms, offering a new strategy for BINOL–metal catalysis based on metal-centered chirality and significantly enhancing the asymmetric synthesis of complex substrates (Scheme 5).

Overall, the development of BINOL-based aluminum catalysts demonstrated that both coordination geometry modulation and steric engineering of the BINOL framework are indispensable for achieving high catalytic performance. Rational ligand design enables precise control over the coordination environment, substrate binding mode, and transition-state organization around the aluminum center, thereby enhancing catalytic activity and stereoselectivity. These studies established BINOL as one of the most versatile ligand platforms for constructing highly efficient chiral aluminum catalysts and provide fundamental principles for the rational design of future asymmetric catalytic systems.



Scheme 4: Catalytic performance validation of hexacoordinated aluminum alkoxide species **5**.



Scheme 5: The mechanism of aluminum complex **5**-catalyzed asymmetric hydroboration of aryl ketones.

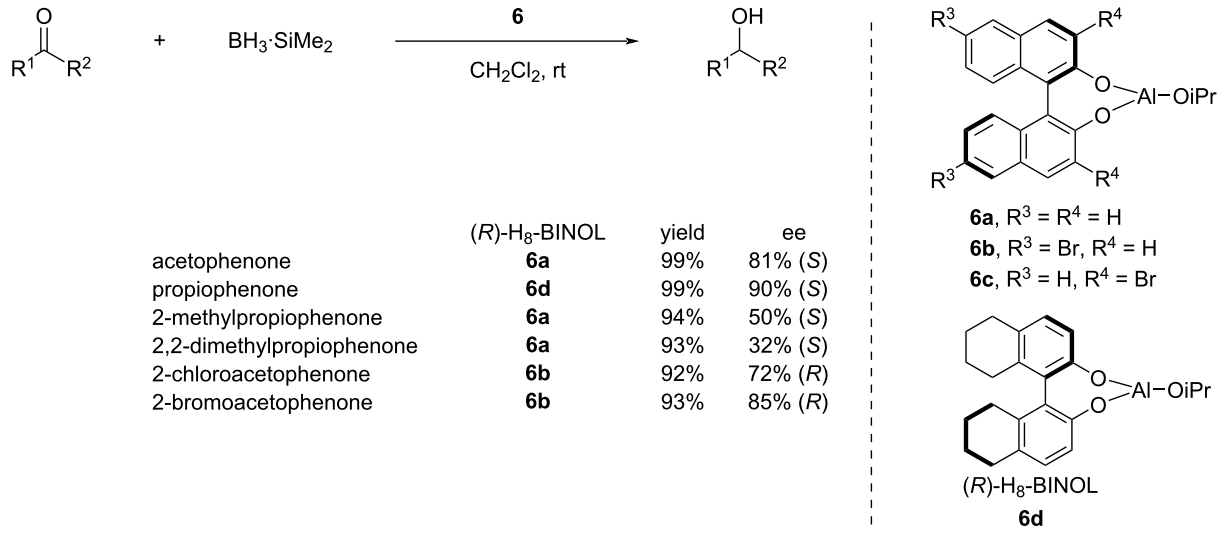
Steric engineering of the BINOL framework

Beyond coordination geometry, the steric environment generated by the BINOL framework plays a decisive role in controlling catalytic selectivity. Structural modifications at the 3,3′-, 6,6′-, and 7,7′-positions have proven particularly effective for regulating substrate approach and transition-state organization [48,49].

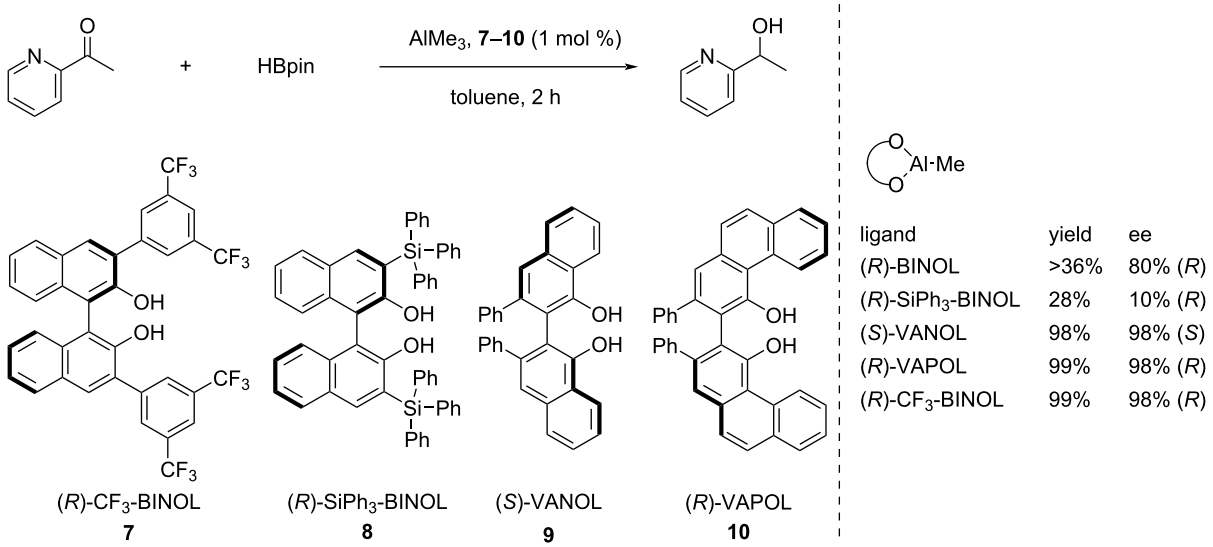
Early investigations demonstrated that subtle modifications of BINOL-derived ligands could dramatically alter stereochemical outcomes in aluminum-catalyzed ketone reductions. Remarkably, changes in ligand substitution patterns not only affected enantioselectivity but also led to inversion of product configuration. These findings provided some of the earliest evidence that steric interactions within the chiral pocket strongly influence the trajectory of hydride delivery. Uang et al. [50] employed chiral BINOL derivatives as ligands in the asymmetric reduction of aromatic ketones. Compared with the unsubstituted complex **6a**, complexes **6b** and **6c** induced an inversion of the absolute configuration, affording (*R*)-configured products, whereas complex **6a** furnished (*S*)-configured products. When complex **6d** was employed, the (*S*)-configuration was obtained with the highest enantioselectivity, reaching an ee value of 90%. The ee values of the corresponding alcohols decreased as the alkyl chain length of the substrates increased, except for phenylacetone, which exhibited the highest ee value in the reduction reaction. In contrast, cyclic ketones displayed a marked decrease in selectivity, likely due to their more rigid conformations. Halogen substituents exerted little influence on the ee value, as did 2-naphthyl and electron-withdrawing nitro groups; however, the presence of electron-donating groups tended to diminish enantioselectivity (Scheme 6).

Subsequent developments focused on expanding the steric profile of the BINOL framework. Rueping et al. [51] employed a series of chiral BINOL-derived ligands **7**–**10** in the asymmetric hydroboration of heteroaryl ketones. This catalytic system was applicable to a broad range of substrates with excellent functional group tolerance. For 2-acetylpyridine substrates, yields reached 99% with ee values of up to 98%. When the substrate scope was extended to aryl-substituted heteroaryl ketones, the use of the bulkier ligands, VANOL (**9**) or VAPOL (**10**), maintained ee values above 95% (Scheme 7). Notably, the resulting 2-heterocyclic alcohols are valuable synthetic intermediates in drug discovery and can also serve as ligands in asymmetric catalysis. Density functional theory (DFT) calculations revealed that the steric hindrance of the optimal ligand ranged from 34% interference with substrate coordination. Furthermore, the ligand could be completely recovered and reused after the reaction, thereby reducing catalyst cost and waste generation in accordance with the principles of green chemistry, making this system particularly suitable for large-scale synthesis.

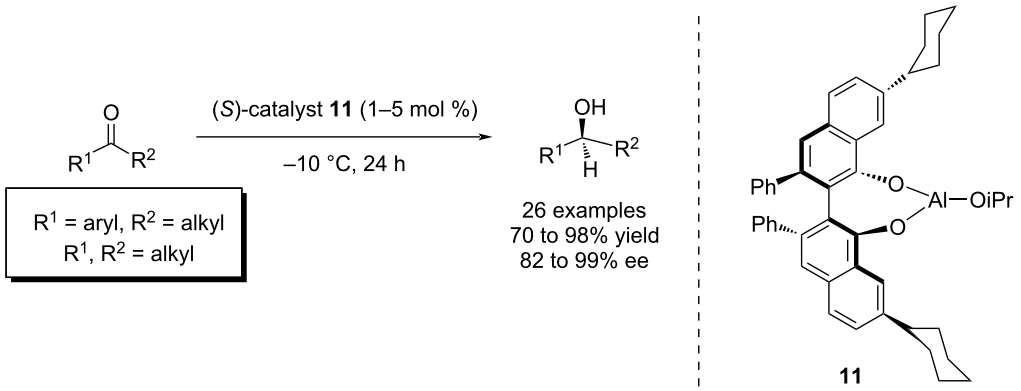
Further evidence for the critical role of steric effects was provided by Wulff and co-workers through the development of 7,7′-dicyclohexyl-substituted VANOL ligands. Wulff et al. [52] developed a catalyst **11** composed of $AlMe_3$ and a 7,7′-dicyclohexyl-substituted VANOL ligand, which was applied to the asymmetric MPV reduction of ketones to efficiently convert them into chiral alcohols. For aromatic ketones, enantioselectivities reached 94 to 99% ee (Scheme 8). The asymmetric MPV reduction of aliphatic ketones was achieved for the first time, affording good enantioselectivities with ee values up to 94%, thereby addressing a gap in this field. The bulky 7,7′-substitu-



Scheme 6: Asymmetric reduction of aromatic ketones catalyzed by organoaluminum compounds **6a–d**.



Scheme 7: Asymmetric hydroboration of heterocyclic ketones catalyzed by organoaluminum compounds containing ligands **7**–**10**.

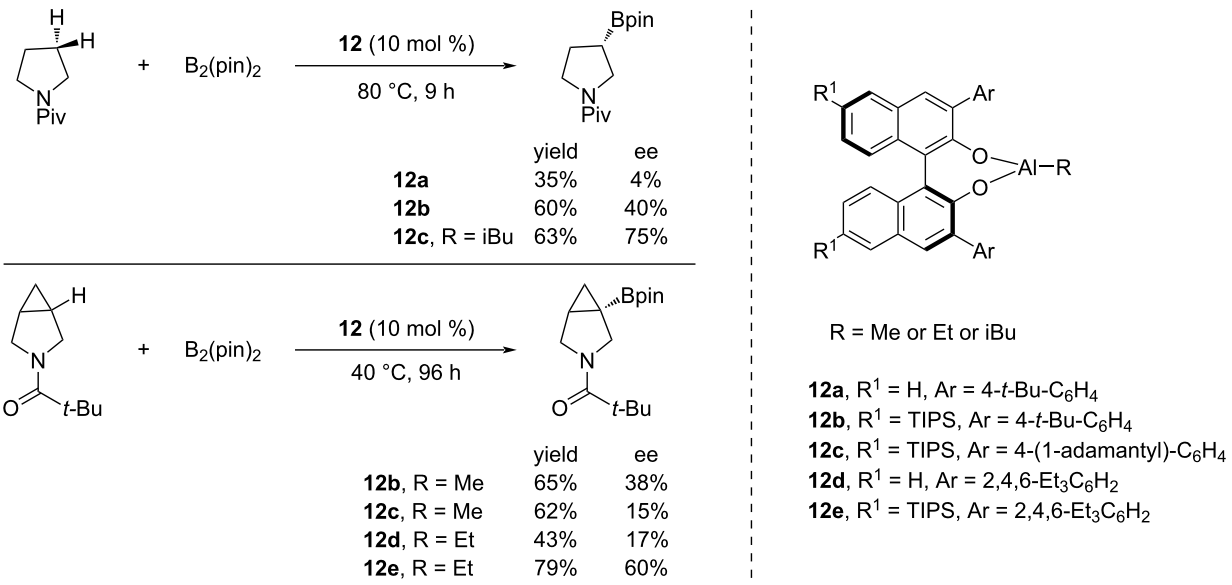


Scheme 8: Asymmetric MPV reduction reactions of ketones catalyzed by organoaluminum compound **11**.

ents of the VANOL ligand outperformed traditional BINOL in aluminum catalysis, confirming their steric control advantage.

An illustrative example of steric modulation through BINOL framework engineering was reported by Nakao and co-workers in the development of a chiral BINOL–Al/Ir cooperative catalytic system for the enantioselective β-C(sp^3)–H borylation of saturated cyclic amines [53]. With catalyst **12a**, the reaction afforded only 4% ee. As the steric bulk of the BINOL framework progressively increased, the stereochemical control of the catalyst was significantly enhanced. The introduction of bulky triisopropylsilyl (TIPS) groups at the 6,6′-positions to afford catalyst **12b** improved the enantioselectivity to up to 40% ee. Further installation of even bulkier 4-(1-adamantyl)phenyl substituents at the 3,3′-positions to generate catalyst **12c** increased the enantioselectivity to as high as 75% (Scheme 9). These results demonstrate that rational steric engineering of the BINOL framework is an effective strategy for enhancing catalytic performance and asymmetric induction.

The same group [54] extended the system (**12b**–**e**) to the bridgehead C–H borylation of 3-azabicyclo[3.1.0]hexane. Modification of the 6,6′-positions of BINOL with TIPS groups enhanced catalyst solubility, enabling a catalyst loading as low as 0.2 mol % and affording up to 62% ee (Scheme 9). This result demonstrated that silyl substitution effectively enhanced both ligand solubility and chiral transfer efficiency at the metal center. This work therefore confirms that rational steric engineering of the BINOL scaffold is a key strategy for enhancing asymmetric induction in cooperative aluminum catalysis.



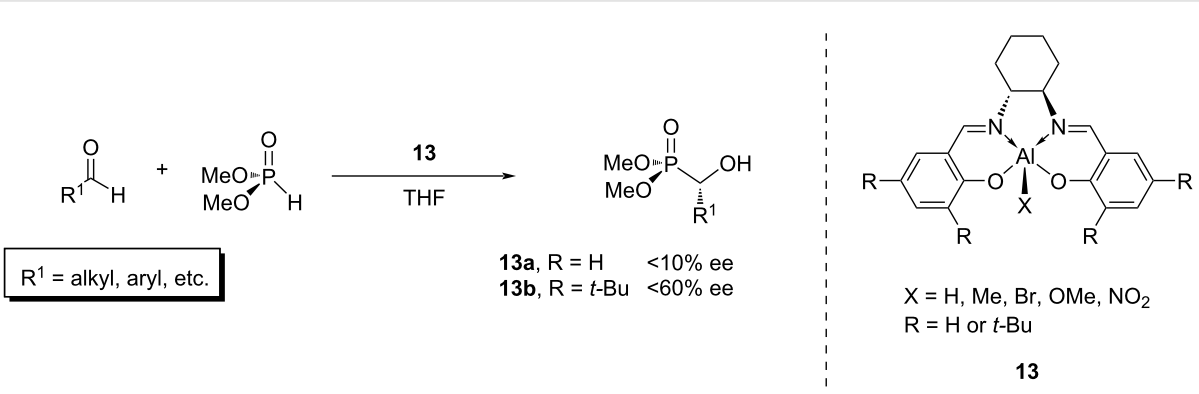
Scheme 9: Aluminum catalysts **12a–c** for the β-C(sp^3)–H borylation reaction and **12b–e** for the bridgehead C–H borylation of 3-azabicyclo[3.1.0]hexane.

Salen-based chiral aluminum catalysts

The term "salen" refers to a class of Schiff bases formed by the condensation of *ortho*-hydroxy-substituted aromatic aldehydes with diamines [55]. Chiral salen aluminum catalysts represent an important class in asymmetric catalysis, and their development has demonstrated the precise tuning of ligand design in conjunction with catalytic performance optimization. Their rigid N_2O_2 framework enables electronic and steric tuning of the aluminum center. Consequently, the catalytic performance of salen aluminum complexes is closely associated with ligand structure and catalyst architecture [56].

Electronic and steric engineering of salen ligands: Electronic and steric modifications of salen ligands provide effective approaches for tuning the Lewis acidity, substrate activation ability, and stereochemical induction of aluminum catalysts [57].

Kee et al. [58] reported chiral salen aluminum catalysts **13** for the asymmetric hydrophosphonylation of aldehydes and demonstrated that subtle ligand modifications exert a profound influence on stereoselectivity. Although both catalysts share the same absolute ligand configuration, catalyst **13a** afforded poor enantioselectivity (<10% ee), whereas the *tert*-butyl-substituted analogue **13b** achieved enantioselectivities of up to approximately 60% ee (Scheme 10). Remarkably, compared with the corresponding salalen systems, the use of catalyst **13b** also led to an inversion of the predominant product configuration, highlighting the decisive role of the ligand steric architecture in controlling the chiral environment around the aluminum center.



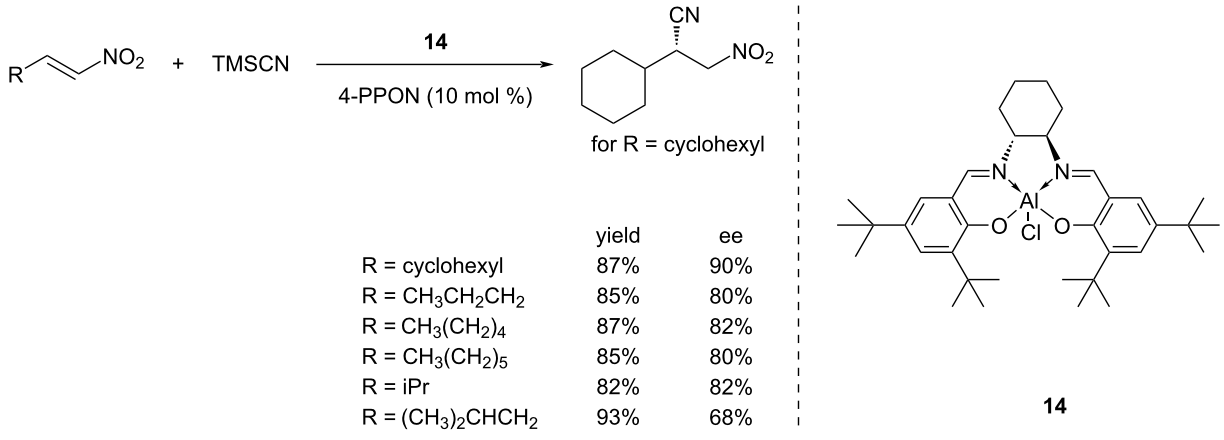
Scheme 10: Aluminum compounds **13** for the hydrophosphonylation of carbonyls.

Khan et al. [59] developed a well-defined chiral Al(III) salen complex **14** as an efficient homogeneous catalyst for the asymmetric hydrocyanation of nitroolefins, with trimethylsilyl cyanide (TMSCN) as the cyanide source and 4-phenylpyridine *N*-oxide (4-PPNO) as a critical additive. Under these optimized conditions, the model substrate (2-nitrovinyl)cyclohexane afforded the corresponding β-nitronitrile with an 87% isolated yield and an excellent enantioselectivity of 90% ee (Scheme 11). Mechanistic studies further demonstrated that 4-PPNO coordinates axially to the aluminum center to form a pentacoordinate species, which not only increases the electrophilicity of the metal center but also facilitates activation of TMSCN. The resulting cooperative interaction between the electron-deficient Al center and the sterically organized salen framework promotes an enantioselective cyanide delivery to the coordinated nitroolefin (Scheme 12). These results demonstrate that the combination of electronic activation through axial coordination and steric confinement provided by the rigid salen scaffold is essential for achieving both high catalytic activity and excellent enantioselectivity in this transformation.

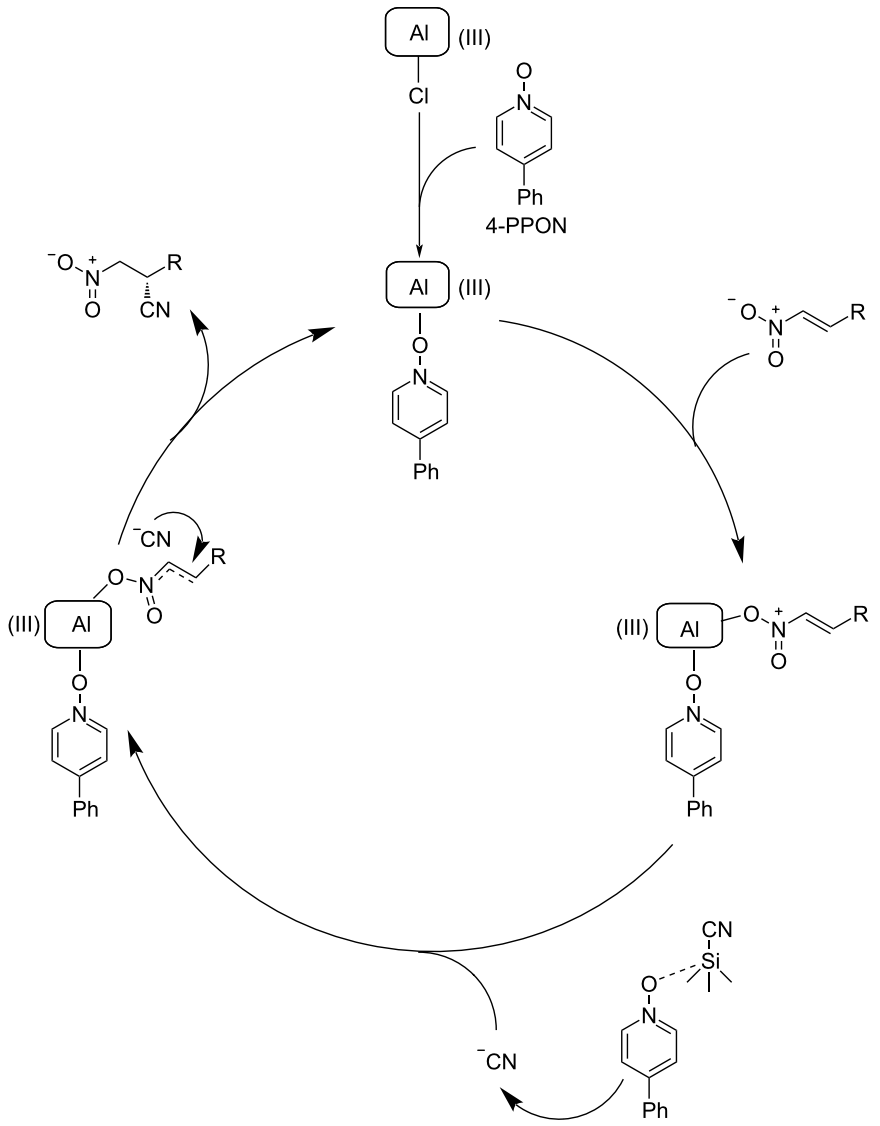
Feijen et al. [60] reported the application of the chiral salen aluminum catalyst **15** in the ring-opening polymerization (ROP) of ε-caprolactone (ε-CL) and its methyl-substituted derivatives. The polymerization rate decreased substantially upon methyl substitution, with ε-CL polymerizing faster than 4-methyl-ε-caprolactone (4-MeCL), which in turn polymerized considerably faster than 6-methyl-ε-caprolactone (6-MeCL). The catalyst exhibited significant stereoselectivity toward 6-MeCL, but no selectivity toward 4-MeCL, indicating that the substituent position influences the stereochemical environment of the active site through steric effects (Scheme 13). This finding provided important guidance for subsequent ligand structure optimization.

Gao, Duan and co-workers. [61] reported (*R*,*R*)-cyclohexanediamine-based chiral salen aluminum complexes for the highly stereoselective polymerization of *rac*-lactide (*rac*-LA). Microstructural analyses of the propylene oxide initiated by these complexes revealed that the chiral salen ligands can effectively control the stereoconformational regularity of the polymer, and that this ability depends on the steric volume of the benzene ring substituents of the auxiliary ligand. Stereoselectivity was markedly enhanced through optimization of the ligand substituents, particularly with the introduction of bulky *tert*-butyl groups and halogen atoms such as chlorine. In toluene at 70 °C, complexes **16a**–**c** catalyzed *rac*-LA to afford isotactic PLA with high P_m and narrow molecular weight distributions (PDI = 1.10–1.22) (Scheme 14). These findings demonstrate that chiral salen aluminum complexes can effectively regulate the stereoconformational regularity of PLA by modulating the electronic effects and steric hindrance of the ligand substituents. Collectively, these studies demonstrated that electronic and steric modulation of salen ligands directly influences Lewis acidity, substrate activation, and stereoselectivity, thereby establishing important structure–activity relationships in salen-based aluminum catalysis.

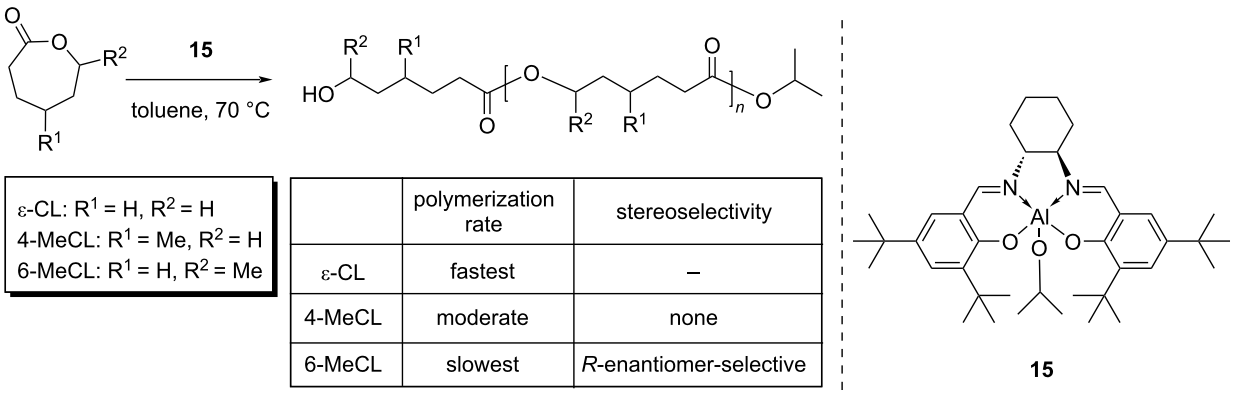
The importance of ligand steric effects was elegantly demonstrated by Evans and co-workers through the development of catalyst **17** for the asymmetric aldol reaction of aldehydes with 5-alkoxyoxazoles [62]. The catalyst incorporates a rigid diaminobinaphthyl-derived salen framework together with bulky 3,5-di-*tert*-butyl substituents, generating a highly confined chiral environment around the aluminum center. The addition of suitable additives enhanced the conversion and allowed for a lower catalyst loading, enabling the efficient synthesis of chiral β-hydroxy-α-amino acid derivatives. The aromatic aldol reaction conducted in toluene with 10 mol % cata-



Scheme 11: Aluminum compound **14** for the asymmetric hydrocyanation of nitroolefins.

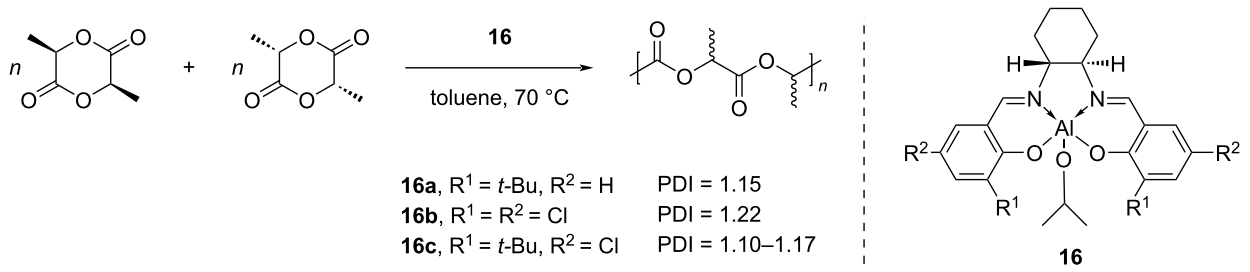


Scheme 12: The mechanism for the asymmetric hydrocyanation of nitroolefins catalyzed by aluminum catalyst **14**.



	polymerization rate	stereoselectivity
ε-CL	fastest	–
4-MeCL	moderate	none
6-MeCL	slowest	*R*-enantiomer-selective

Scheme 13: Aluminum compound **15** for the ROP of ε-CL and its methyl derivatives.



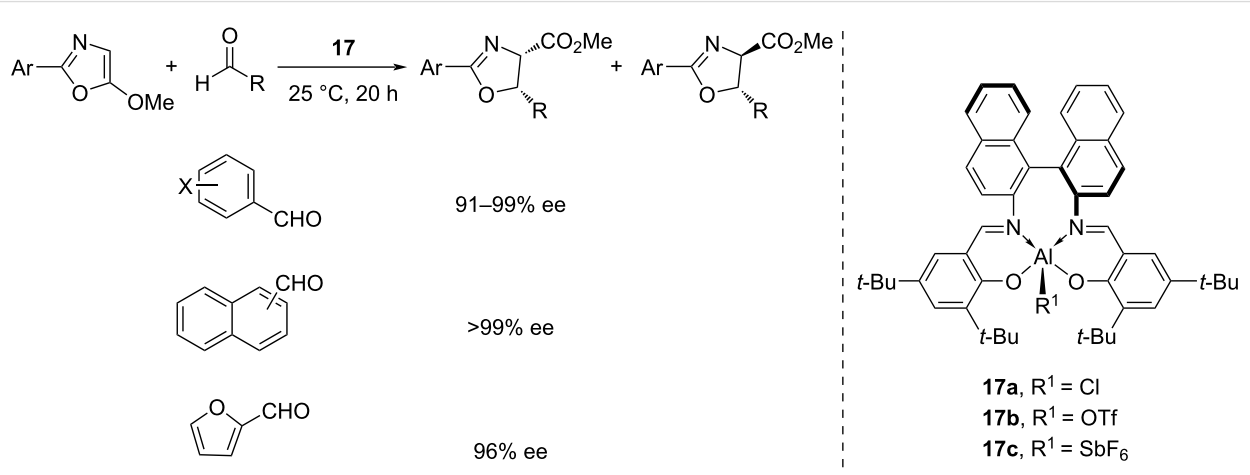
Scheme 14: Aluminum compounds **16** for *rac*-LA polymerization reactions.

lyst and 20 mol % $LiClO_4$ as an additive afforded the *cis*-oxazoline product in 90–99% yield and 91–99% ee (Scheme 15). These results demonstrate that precise steric tuning of the ligand framework can significantly enhance stereochemical control by regulating substrate orientation and transition-state organization around the aluminum center.

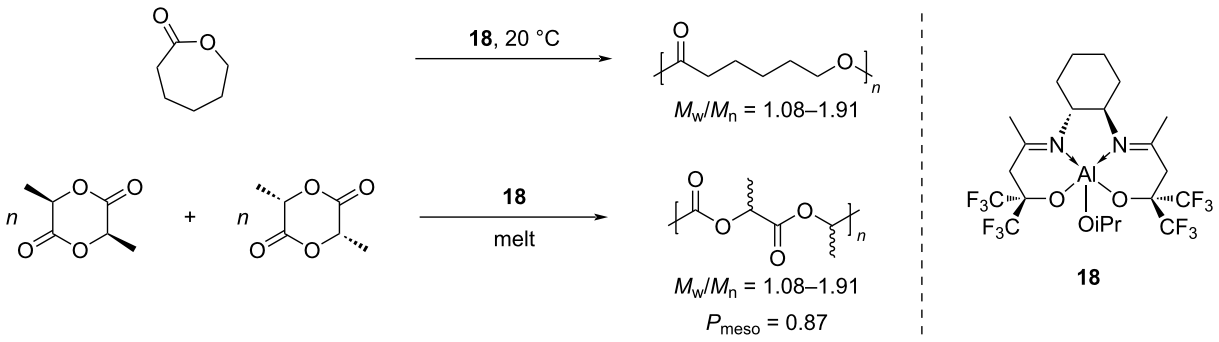
Catalyst architecture engineering: Beyond ligand modification, engineering the overall catalyst architecture has emerged as another effective strategy for regulating the coordination environment and catalytic behavior of salen aluminum complexes [63]. Structural variations such as supported catalysts, multinuclear systems, and expanded ligand frameworks can significantly influence substrate binding modes, monomer insertion pathways, and catalytic selectivity [64].

Carpentier et al. [65] developed the fluorinated dialkoxy-diimino aluminum complex **18** as structurally modified analog for traditional salen systems. Unlike classical salen ligands, where rigid phenolate rings generally enforce a square-pyramidal coordination geometry, replacement of the phenolate units with sp^3-hybridized fluorinated alkoxide donors significantly increased the ligand flexibility, leading to distorted trigonal-bipyramidal aluminum centers. This backbone transformation altered the steric environment and coordination mode around the metal center, thereby affecting monomer activation and stereocontrol during polymerization. The AlOiPr complex **18** is an effective initiator for the ROP of ε-CL and *rac*-LA, giving polymers with high molecular weights and relatively narrow polydispersities (M_w/M_n = 1.08–1.91). The PLAs produced, both under slurry and melt conditions, with chiral complex **18**, have a highly isotactic-enriched stereoblock microstructure (P_{meso} = 0.87) (Scheme 16). Notably, both achiral and chiral ligand backbones generated similar levels of isotactic enrichment, indicating that the coordination geometry and backbone flexibility, rather than backbone chirality alone, played a decisive role in controlling the stereoselectivity. These results demonstrate that a modification of the salen framework can profoundly influence the catalyst structure and polymerization behavior by regulating aluminum coordination geometry and ligand flexibility.

Weck and Madhavan [66] reported a landmark study on polymer-supported salen aluminum catalysts. The (*R*,*R*)-



Scheme 15: Aluminum compounds **17** for asymmetric aldol reactions of aldehydes and 5-alkoxyoxazoles.

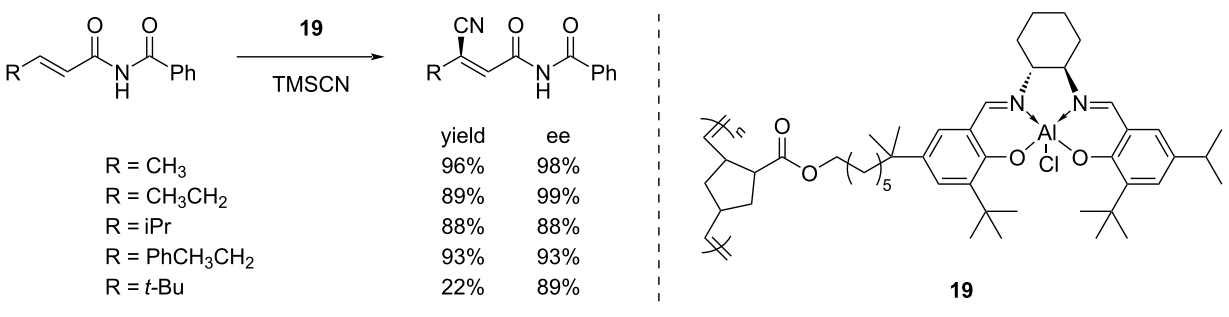


Scheme 16: Aluminum compound **18** for ε-LA and *rac*-LA polymerization reactions.

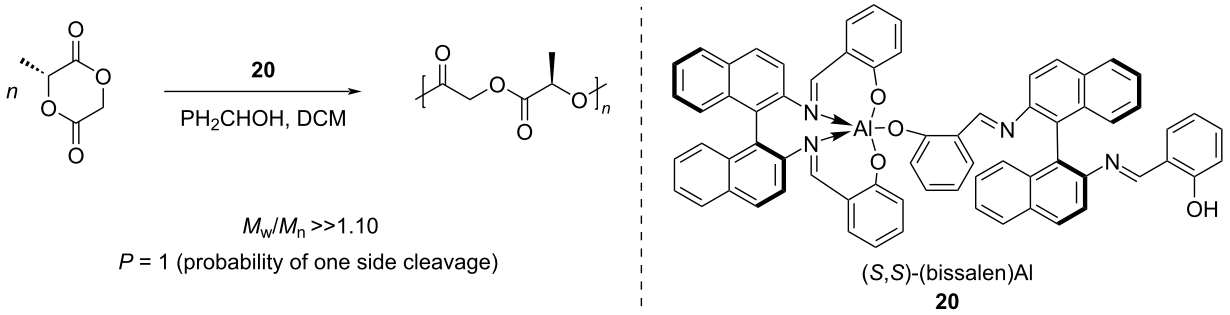
salen–AlCl complex was immobilized on a polynorbornene scaffold to afford catalyst **19**, which was successfully applied in the asymmetric 1,4-conjugate addition of α,β-unsaturated imides with cyanide. The catalytic system retained the excellent stereoselectivity of traditional homogeneous salen–Al catalysts, achieving enantioselectivities of 88–99% ee (Scheme 17). Several breakthrough advances were realized, including the reduction of catalyst loading from the conventional 10–15 mol % to 5 mol % and a 50–66% decrease in metal usage while maintaining reaction efficiency, thereby demonstrating the unique advantages of polymer-supported strategies in salen–Al catalysis. These findings demonstrated that the modification of the catalyst architecture at the macromolecular level can influence catalytic performance by regulating catalyst-site proximity and cooperative interactions, providing an effective strategy to enhance activity without altering the intrinsic chiral salen–Al active site.

More recently, Wang et al. [67] developed a chiral (bissalen)Al complex **20**, achieving significant advances in both regio- and stereoselectivity control. Compared with conventional monosalen systems, the bissalen framework provided a more ordered coordination environment and enhanced cooperative effects between catalytic sites. The catalyst efficiently promoted the ROP of 3-methyl glycolide (MeG) with regioselectivity exceeding 99%, enabling the successful synthesis of fully alternating poly(lactic-*co*-glycolic acid) (PLGA) with properties superior to conventional non-alternating or partially alternating PLGA (Scheme 18). Mechanistic studies indicated that the bissalen framework creates a more confined chiral environment, improving discrimination between competing reaction sites and promoting selective glycolyl-site activation. The proposed mechanism was investigated using the enantiomeric (*R*,*R*)-configured aluminum alkoxide model and (*S*)-MeG. Coordination of MeG to the aluminum center proceeds through TS1, followed by nucleophilic attack of the Al-bound alkoxide to form Int1 and the more stable intermediate Int2. Subsequent dissociation of the carbonyl oxygen from the aluminum center and cleavage of the acyl C–O bond through TS2 generate the ring-opened propagating species Int3, which can undergo subsequent monomer insertion (Scheme 19). These results demonstrate that expansion of the ligand framework from monosalen to bissalen can profoundly influence catalytic behavior by tailoring the spatial organization of the coordination sphere and strengthening substrate recognition at the aluminum center.

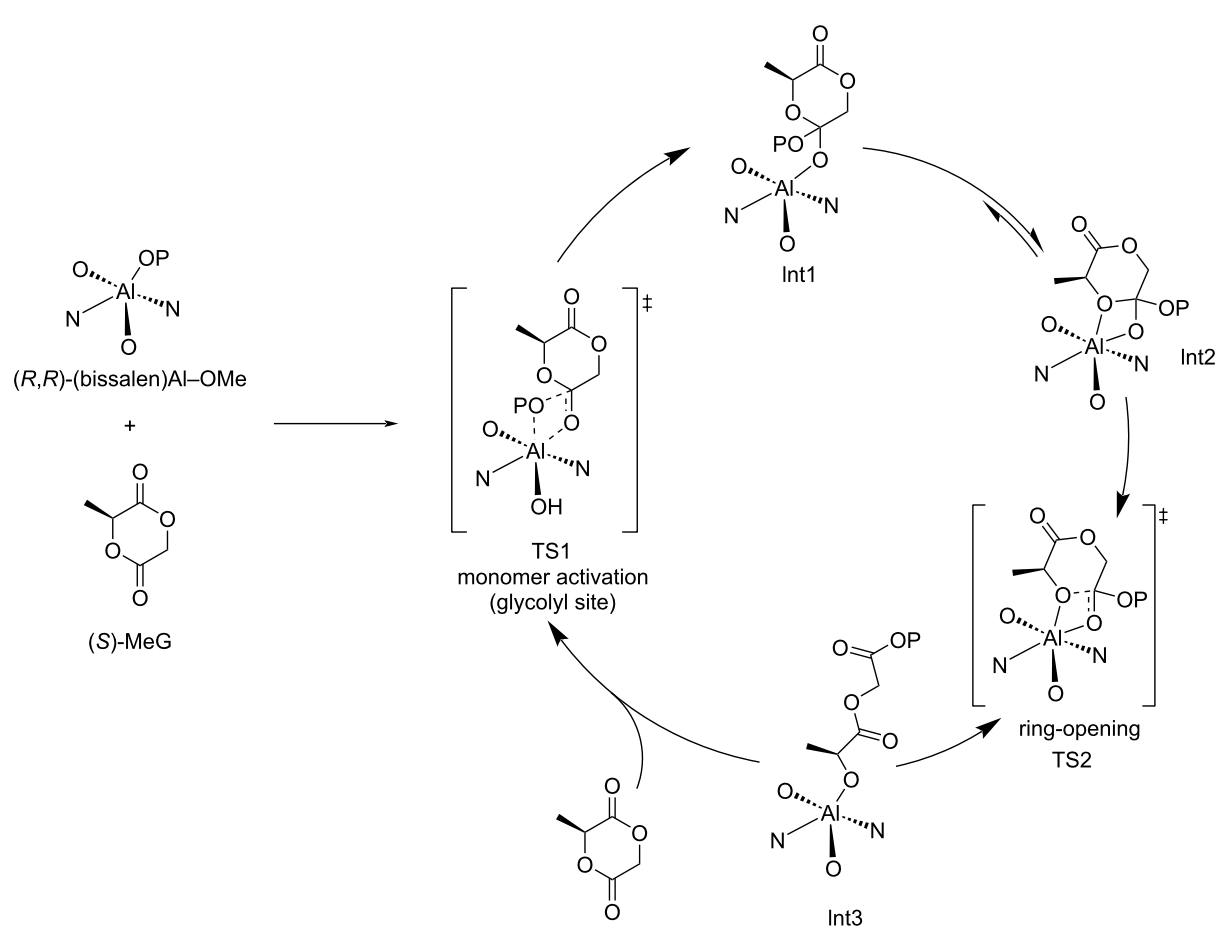
Overall, the development of salen-based aluminum catalysts demonstrated that both ligand-level modulation and catalyst



Scheme 17: Aluminum compound **19** for asymmetric 1,4-conjugate addition reaction of α,β-unsaturated imides with cyanides.



Scheme 18: Aluminum compound **20** for ROP of MeG.



Scheme 19: Proposed ring-opening pathway of (*S*)-MeG mediated by an (*R*,*R*)-configured (bissalen)Al alkoxide model. TS and Int denote transition state and intermediate, respectively, and OP- represents the propagating polymer chain.

architecture engineering are crucial for achieving high catalytic performance. Electronic and steric effects govern Lewis acidity and stereochemical induction, whereas catalyst architecture determines coordination environments and substrate activation modes. The interplay of these factors ultimately dictates the catalytic activity, regioselectivity, and enantioselectivity, providing valuable guidelines for the rational design of next-generation chiral aluminum catalysts.

N-Heterocycle-supported chiral aluminum catalysts: Since the 1990s, nitrogen-containing heterocyclic ligands have demonstrated unique stereocontrol capabilities in chiral aluminum catalyst design, with their rigid frameworks and multiden-

tate coordination features opening new avenues for asymmetric catalysis [68-70].

Steric and electronic engineering of N-heterocyclic ligands: The catalytic performance of N-heterocycle-supported aluminum catalysts is strongly influenced by the steric and electronic properties of the ligand framework. Systematic ligand modification has revealed clear structure–activity relationships that govern catalytic activity, stereoselectivity, and polymer microstructure [71,72].

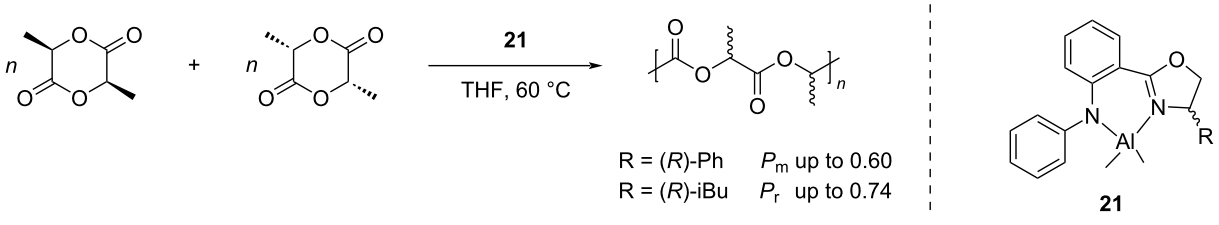
Du et al. [36] synthesized and characterized a series of aluminum complexes **21** containing chiral bidentate anilino-oxazoline ligands and investigated their catalytic properties in the ROP of *rac*-LA. By systematically varying the substituents on the ligands, the study achieved precise modulation of both the reactivity and stereoselectivity of the aluminum catalysts in the ROP of *rac*-LA. The optimal homoselectivity (P_m = 0.60) and heteroselectivity (P_r = 0.74) were obtained under specific substituent conditions (Scheme 20). The oxazoline ring serves as the chiral core, and the electronic and steric effects of its substituents are key factors governing the polymerization behavior.

Similarly, Liu and Ma [73] reported a series of dimethylaluminum complexes **22** bearing bidentate *N*-[2-(1-piperidinyl)benzyl]anilino-type ligands. These complexes effectively initiated the ROP of *rac*-LA without an external initiator, exhibiting good controllability and a narrow molecular weight distribution of the resulting polylactide (PDI = 1.06–1.18) (Scheme 21). Steric hindrance from *ortho*-substituents on the aniline moiety reduced catalytic activity, whereas electron-withdrawing substituents at the *meta* or *para*-positions enhanced activity by increasing the electrophilicity of the metal center. Terminal group analysis suggested that the polymerization proceeded via a coordination–insertion mechanism involving monomer insertion into the Al–N(amido) bond. The amido-initiated polymerization exhibited characteristics comparable to those initiated by conventional aluminum alkoxide active species, offering a new strategy for polylactide synthesis.

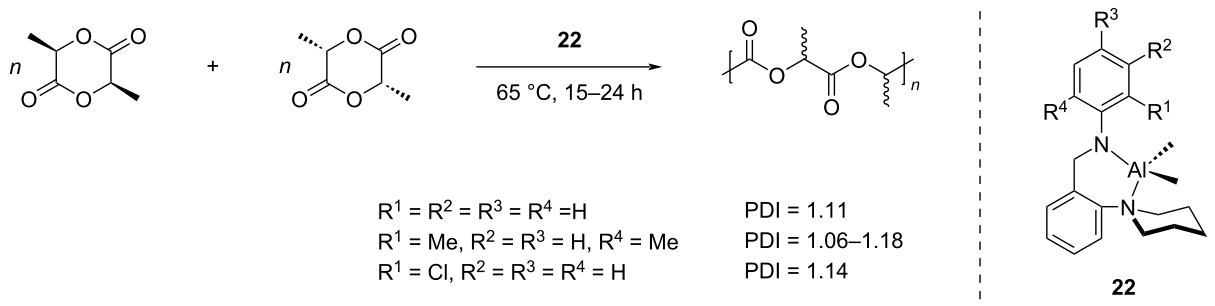
Steric effects were further demonstrated by Vidović and co-workers [74]. Their chiral oxazoline-containing β-diketiminate aluminum complexes **23** possess structurally differentiated achiral and chiral termini. Systematic enlargement of the steric bulk at the achiral terminus significantly improved the enantioselectivity of the asymmetric Diels–Alder reaction between chalcone and 1,3-cyclohexadiene. At the chiral oxazoline site, catalysts bearing *tert*-butyl substituents provided the optimal steric shielding and achieved the highest enantioselectivity (up to 68% ee) (Scheme 22). However, excessive steric congestion adversely affected substrate coordination and reduced the catalytic efficiency. These observations emphasize that a carefully tuned steric confinement, rather than simply maximizing steric bulk, is crucial for achieving effective stereocontrol.

Ligand coordination modulation and mechanisms: The coordination environment surrounding the aluminum center is a key factor governing catalytic activity and stereoselectivity in N-heterocycle-supported aluminum catalysts. Owing to the versatile coordination modes of nitrogen-containing ligands, aluminum complexes can adopt diverse coordination geometries and nuclearities, enabling precise regulation of substrate activation and stereochemical induction [75,76].

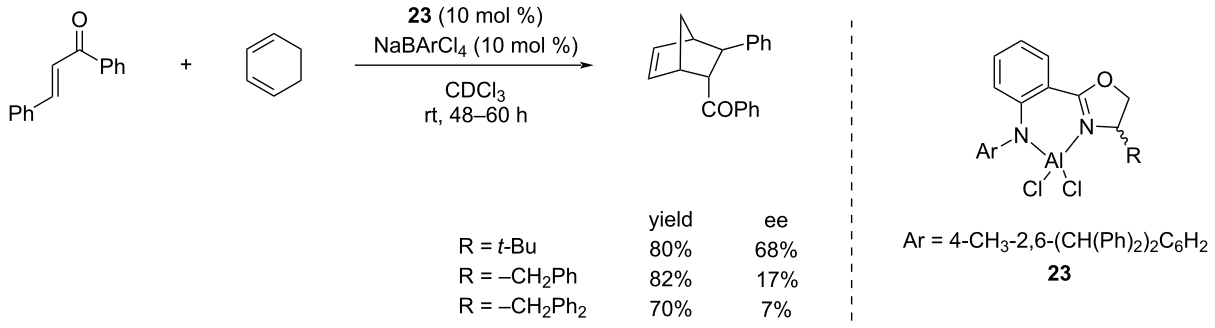
Liu and Wei [77] demonstrated the important role of a ligand-controlled coordination environment modulation through chiral pyrrolylimine- and pyrrolylamine-derived aluminum complexes **24** and **25**. Depending on the ligand's donor framework, the reaction with trimethylaluminum afforded either a hexacoordinate tris-ligated aluminum complex **24** or a tetracoordinate monoligated dialkylaluminum complex **25**, both of which were subsequently applied to the polymerization of *rac*-LA (Scheme 23). The resulting differences in coordination architecture altered the steric environment and coordination saturation around the aluminum center, leading to variations in catalytic activity and the molecular weights of the resulting polymers. Although both complexes exhibited a preference for the formation of isotactic-rich poly(lactic acid) (PLA), their distinct coordination modes gave rise to different polymerization performances, underscoring the critical role of ligand-induced



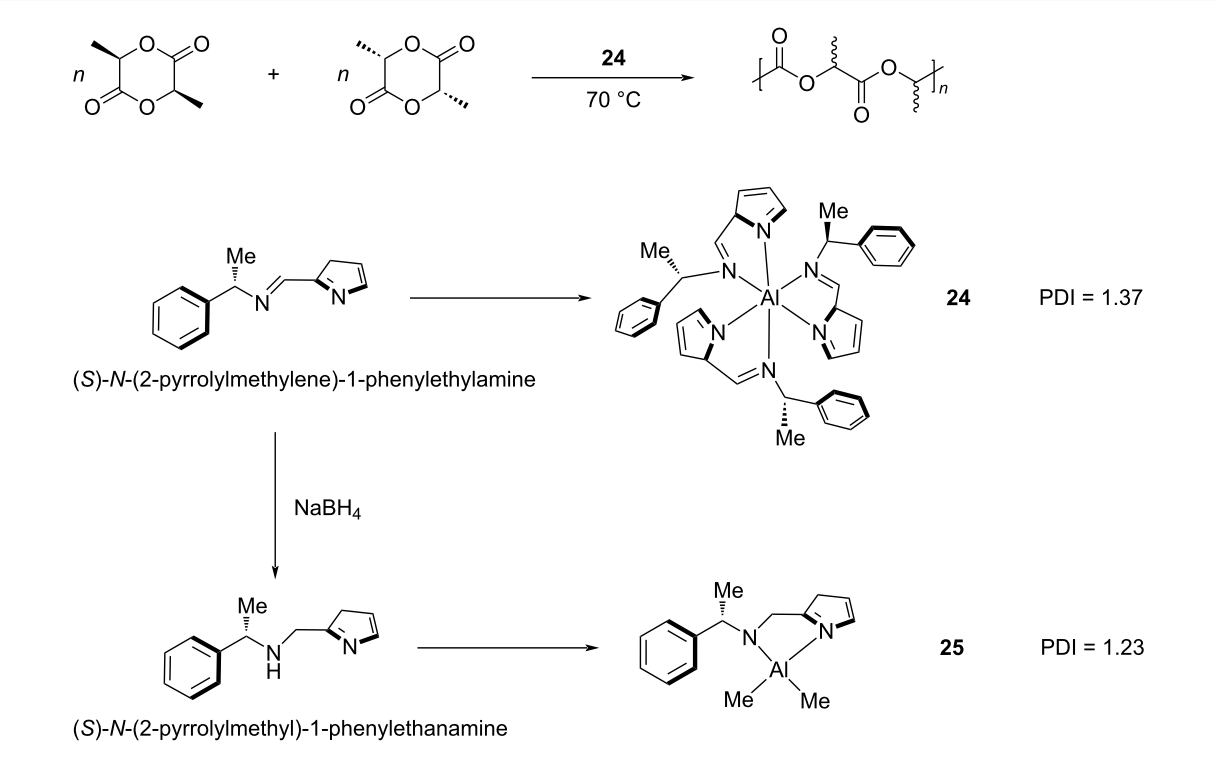
Scheme 20: Aluminum compounds **21** for *rac*-LA polymerization reactions.



Scheme 21: Aluminum compounds **22** for *rac*-LA polymerization reaction.



Scheme 22: Aluminum compounds **23** for asymmetric Diels–Alder cycloaddition reactions.



Scheme 23: Aluminum complexes **24** and **25** for *rac*-LA polymerization reaction.

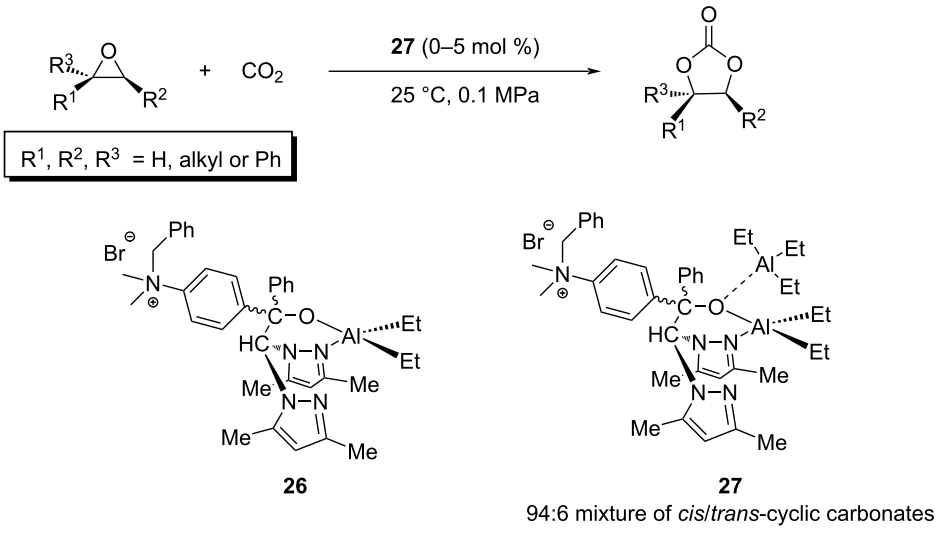
coordination environment modulation in regulating the behavior of aluminum catalysts.

Further advances were achieved through ligand-controlled coordination modulation in multinuclear aluminum systems. North et al. [78] designed a chiral NNO-type heteroscorpionate ligand that reacts with trialkylaluminum in either a 1:1 or 1:2 stoichiometric ratio selectively affording mononuclear complex **26** or dinuclear complex **27** (Scheme 24). This ligand-directed assembly enables precise regulation of the aluminum nuclearity and coordination environment. More importantly, the dinuclear architecture promotes cooperative interactions between adjacent aluminum centers and facilitates bifunctional activation during catalysis, leading to enhanced activity in the cycloaddition of epoxides with CO_2. Mechanistic studies further suggested that the bridged dinuclear framework favors intramolecular cooperative catalysis and stabilizes key intermediates, demonstrating that ligand-controlled coordination modes can directly influence the catalytic pathway and reaction efficiency (Scheme 25).

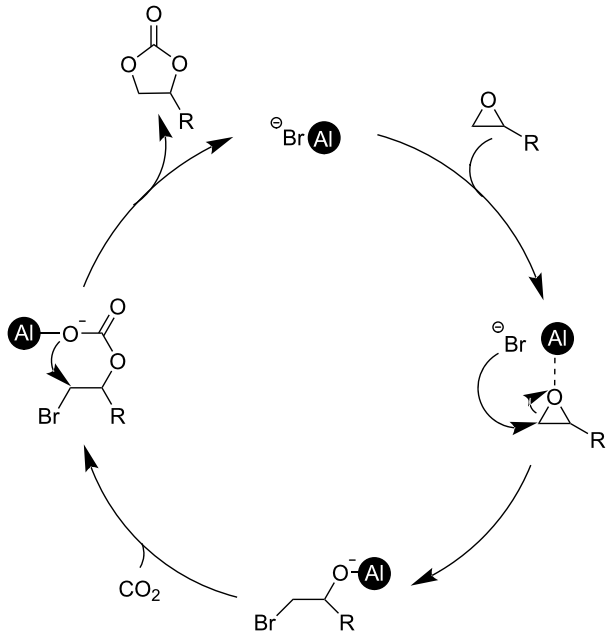
Kol et al. [79] developed an aluminum complex **28** based on a bipyrrolidinyl-salan ligand, in which the ligand adopts a highly preorganized pentacoordinate conformation around the aluminum center due to the incorporation of the rigid C_2-symmetric bipyrrolidinyl core and an adjacent aryl substituent. The resulting steric hindrance significantly enhanced the stereocontrol ability of the catalyst. For *rac*-LA, the enantiopure catalysts exhibited low activity and produced atactic polymers, whereas the racemic catalysts displayed high activity and afforded heterotactic PLA (P_r = 0.99) through chain-end group exchange between mismatched enantiomers (Scheme 26). Mechanistic investigations revealed that a rapid polymer-chain exchange between opposite catalyst enantiomers effectively alleviates the stereochemical mismatch between the growing polymer chain and the incoming monomer. This dynamic coordination process serves as the origin of the remarkable heteroselectivity, highlighting the important role of coordination dynamics in stereocontrolled polymerizations.

Subsequently, the same group [80] reported chiral aluminum catalysts **29** based on tetradentate (ONNO) salanol ligands. Catalyst **29a** catalyzed the *meso*-lactide (*meso*-LA) polymerization to yield highly syndiotactic PLA (P_s = 0.92), whereas catalyst **29b** showed high heterotactic selectivity toward *meso*-LA with P_r = 0.89 (Scheme 27). The ligands' bispyrrolidine core, owing to its rigid chiral structure, enforced a defined wrapping around the aluminum center, ensuring the complex existed as a single stereoisomer and preventing the formation of diastereomeric mixtures, thereby achieving high stereoselectivity in polymerization. This study further demonstrates that controlling the coordination geometry of multidentate N-heterocyclic ligands represents an effective strategy for achieving a highly selective stereocontrolled polymerization.

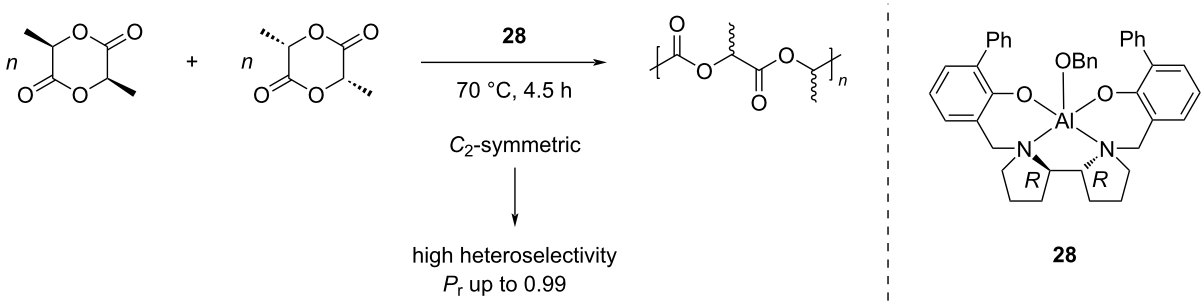
Overall, N-heterocycle-supported aluminum catalysts highlight the critical roles of both ligand steric/electronic properties and coordination environment modulation in determining catalytic performance. The versatile coordination modes and structural diversity of nitrogen-containing ligands enable fine control over Lewis acidity, substrate activation, stereochemical induction, and cooperative effects between aluminum centers. Conse-



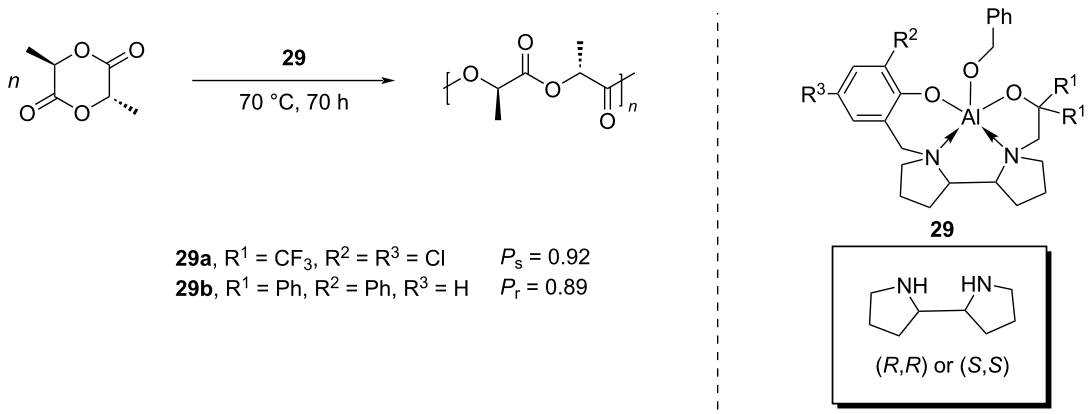
Scheme 24: Structural comparison of monoaluminum complex **26** and dinuclear aluminum cooperative catalyst **27**, and the CO_2 cycloaddition to epoxides catalyzed by compound **27**.



Scheme 25: Mechanism of the CO_2 addition to epoxides catalyzed by aluminum catalyst **27**.



Scheme 26: Aluminum compound **28** for *rac*-LA polymerization reaction.



Scheme 27: Aluminum compounds **29** for the *meso*-LA polymerization reaction.

quently, rational engineering of N-heterocyclic frameworks provides an effective strategy for tailoring catalytic activity, regioselectivity, and stereoselectivity, further expanding the scope of chiral aluminum asymmetric catalysis.

Other types of chiral aluminum catalysts: In addition to the dominant BINOL, salen, and nitrogen-based ligand frameworks, a variety of other chiral ligand systems have been explored to diversify aluminum-catalyzed asymmetric transformations. These alternative ligands provide complementary steric and electronic environments, expanding the structural and functional repertoire of aluminum catalysts beyond the well-established classes. This section highlights these less conventional systems and illustrates how they complement the major ligand families discussed earlier.

Chiral sulfur-containing ligands represent one such class of alternative donor motifs. Node et al. [81] applied aluminum complex **30** obtained with these ligands in a tandem Michael addition/MPV reduction reaction, achieving high enantioselectivity for α,β-unsaturated ketones and allylic alcohols. For styrene-derived substrates, the reductions gave the products with 96–98% ee, demonstrating that sulfur coordination can effectively induce asymmetry in aluminum-catalyzed reactions (Scheme 28). These results showed that donor atoms beyond oxygen and nitrogen can provide efficient stereocontrol, emphasizing the flexibility of aluminum coordination chemistry.

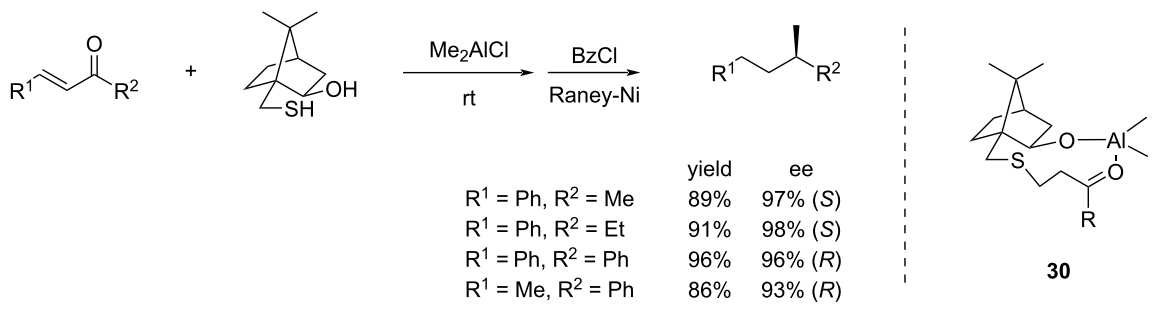
Renaud and Corminboeuf [82] employed compound **31** obtained from the TADDOL ligand 2,2-dimethyl-α,α,α',α'-tetra-1-naphthalenyl-1,3-dioxolan-4,5-dimethanol and triisobutylaluminum in the Diels–Alder reaction of cyclopentadiene with *N*-alkoxyacrylamides, achieving enantioselectivities up to 92% (Scheme 29).

Later, Hori, Mino and co-workers [83] used the TADDOL-Al catalyst **32** for the kinetic resolution of racemic citronellal, illustrating that TADDOL ligands can modulate substrate orientation and reactivity even under challenging conditions. Compared to BINOL, TADDOL's higher conformational flexibility reduces its spatial recognition, leading to a much lower enantioselectivity (20% ee) (Scheme 30). Nonetheless, its immense steric hindrance uniquely suppresses side reactions by preventing product-induced ligand substitution at aluminum. These results showed that balancing TADDOL's rigidity and flexibility can precisely modulate substrate orientation and catalytic activity, guiding the design of challenging asymmetric reactions.

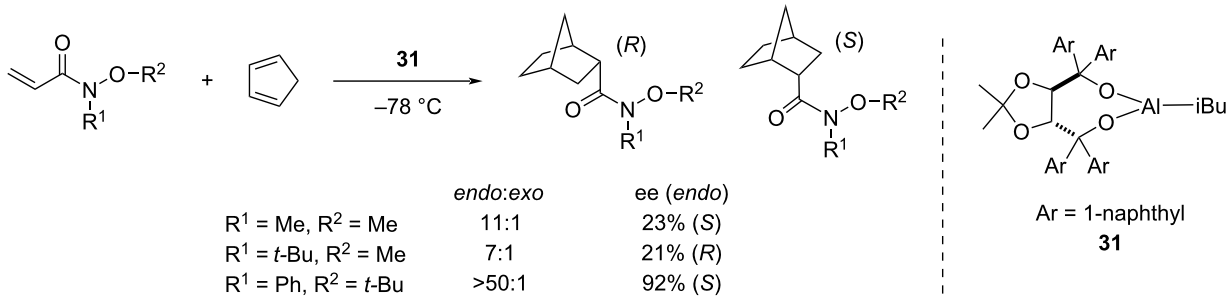
Diamine-supported aluminum catalysts provide another distinct strategy for asymmetric induction. Maruoka et al. [84] applied chiral diamine-aluminum complex **33** to the rearrangement of α,α-disubstituted α-aminoaldehydes. This reaction delivered excellent enantioselectivity up to 97% ee, affording optically active α-hydroxyketones after acidic hydrolysis (Scheme 31). The study highlights the utility of bidentate nitrogen ligands in extending the mechanistic and structural diversity of aluminum-catalyzed transformations, complementing both salen and oxazoline systems.

Phosphite ligands constitute an additional alternative for aluminum-catalyzed asymmetric reactions. Nandi, Katz and co-workers [85] reported aluminum complexes **34** bearing axially chiral vaulted hemispherical calix[4]arene phosphite ligands for the asymmetric MPV reduction of substituted acetophenones (Scheme 32). Using achiral isopropanol as the hydride source, the optimized catalyst afforded up to 99% ee in the reduction of *o*-fluoroacetophenone, demonstrating the effectiveness of this ligand framework for a highly enantioselective MPV reduction.

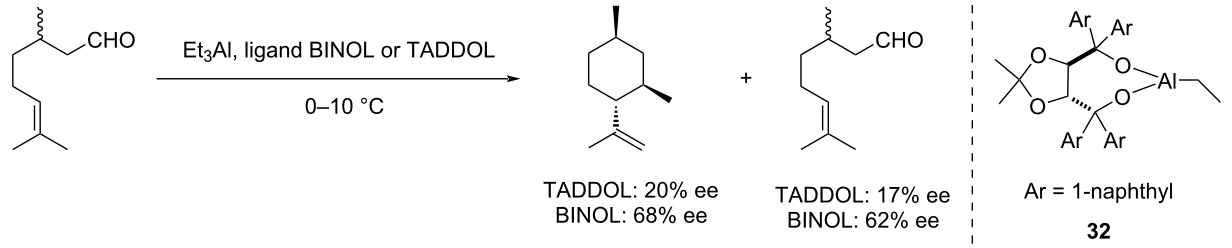
Overall, these alternative ligand frameworks demonstrate that efficient chiral aluminum catalysis is not limited to BINOL-, salen-, or N-heterocycle-based systems. By introducing diverse donor atoms and structural motifs, including sulfur-, oxygen-,



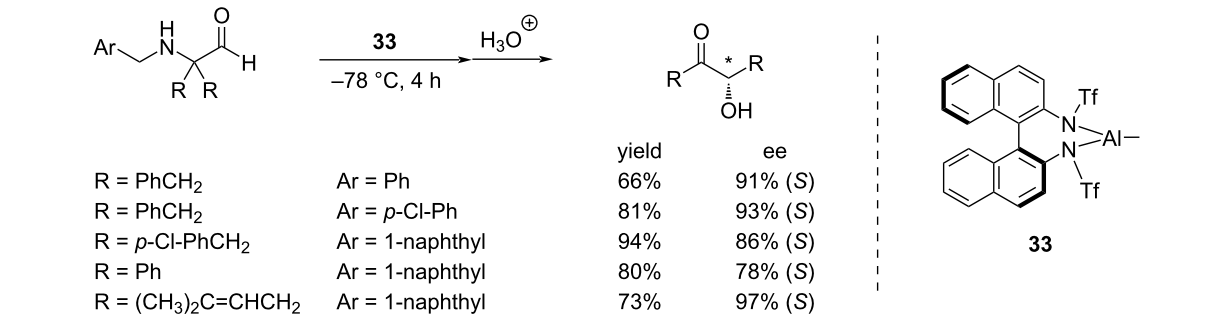
Scheme 28: Aluminum compounds **30** applied to a tandem Michael addition/MPV reaction.



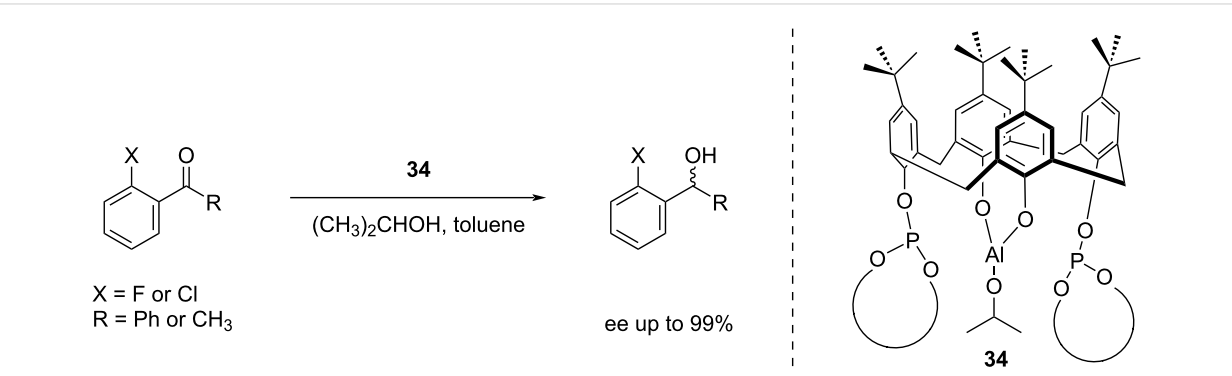
Scheme 29: Aluminum compound **31** for the Diels–Alder reaction of cyclopentadiene with *N*-alkoxyacrylamides.



Scheme 30: Aluminum compound **32** for the kinetic resolution of racemic citronellal.



Scheme 31: Aluminum compound **33** for the rearrangement of α,α-disubstituted α-aminoaldehydes.



Scheme 32: Aluminum compound **34** for the asymmetric MPV reduction of substituted acetophenones.

nitrogen-, and phosphorus-containing ligands, researchers have further expanded the coordination chemistry and stereocontrol strategies available for aluminum catalysts. These studies highlight the versatility of aluminum in accommodating structurally distinct chiral ligands and provide valuable inspiration for the development of next-generation asymmetric catalytic systems with broader substrate scope and improved catalytic performance.

Conclusion

Chiral aluminum catalysts have proven to be powerful tools for asymmetric catalysis, enabling precise stereocontrol in cycloadditions, MPV reductions, ring-opening polymerizations and other key transformations. Based on BINOL, salen and N-heterocyclic scaffolds, rational ligand design achieves efficient coordination modulation of aluminum centers, precisely tuning their coordination geometry, Lewis acidity and chiral microenvironment, while establishing clear structure–activity relationships between catalyst structures and catalytic performance – this forms the core of chiral aluminum catalyst development. Compared with traditional transition-metal catalysts, aluminum-based systems offer inherent advantages of high earth abundance, low toxicity and cost-effectiveness, with tunable ligand architectures lending unique potential for stereoselectivity optimization.

Notwithstanding these advances, notable challenges remain: limited substrate scope, suboptimal stereocontrol for sterically or electronically demanding substrates, difficulties in catalyst recovery and recyclability, and incompletely elucidated structure–activity relationships for some novel systems, all of which restrict their application in complex molecular synthesis and industrial scale-up. Future research should focus on designing novel ligand frameworks to diversify aluminum center coordination modulation strategies, clarifying structure–activity relationships via integrated experimental and theoretical approaches, and incorporating green strategies such as catalyst immobilization to boost catalytic efficiency and recyclability.

By leveraging the intrinsic structural flexibility and tunable coordination properties of aluminum centers, synergistic optimization of ligand design, coordination modulation and structure–activity relationship will drive the development of high-performance chiral aluminum catalysts with excellent regio- and stereoselectivity. Sustained innovation in this field will further expand the utility of aluminum catalysts in the synthesis of pharmaceuticals, fine chemicals and functional materials, establishing them as an economical, environmentally benign alternative to conventional transition-metal catalysts and advancing sustainable asymmetric catalysis.

List of Abbreviations

The abbreviations used in the text and schemes are collected in Table 1.

Table 1: Abbreviations.

4-MeCL	4-methyl-ε-caprolactone
4-PPNO	4-phenylpyridine *N*-oxide
6-MeCL	6-methyl-ε-caprolactone
BINOL	1,1'-binaphthyl-2,2'-diol
CF_3-BINOL	trifluoromethyl-substituted 1,1'-binaphthyl-2,2'-diol
DCM	dichloromethane
DFT	density functional theory
DPP-H_8-BINOL	partially hydrogenated diphenyl-substituted BINOL
ee	enantiomeric excess
HBpin	pinacolborane
MeG	3-methyl glycolide
meso-LA	*meso*-lactide
MPV	Meerwein–Ponndorf–Verley
M_w	weight-average molecular weight
M_n	number-average molecular weight
PDI	polydispersity index
PLA	poly(lactic acid)
PLGA	poly(lactic-*co*-glycolic acid)
P_m	probability of *meso* dyad formation
P_r	probability of racemic dyad formation
P_s	probability of syndiotactic placement
rac-LA	*rac*-lactide
ROP	ring-opening polymerization
salan	saturated salen ligand
salalen	partially hydrogenated salen ligand containing one imine and one amine donor
salen	*N*,*N*′-bis(salicylidene)ethylenediamine
TADDOL	2,2-dimethyl-α,α,α′,α′-tetraaryl-1,3-dioxolane-4,5-dimethanol
TIPS	triisopropylsilyl
TMSCN	trimethylsilyl cyanide
VANOL	4,6-diphenyl-3-hydroxy-2-naphthoic acid-derived axially chiral biaryl ligand
VAPOL	vaulted biphenanthrol
ε-CL	ε-caprolactone

Funding

We gratefully acknowledge financial support from the Beijing Natural Science Foundation (2252021).

Author Contributions

Tianzhe Wen: conceptualization; formal analysis; investigation; methodology; validation; visualization; writing – original draft. Xiaoli Ma: formal analysis; funding acquisition; project administration; resources. Ziyuan Pang: data curation; formal analy-

sis; supervision. Xiaobo Yang: investigation; resources; writing – review & editing. Zhi Yang: conceptualization; funding acquisition; project administration; writing – review & editing.

ORCID® iDs

Xiaoli Ma - https://orcid.org/0000-0003-2632-5367

Data Availability Statement

Data sharing is not applicable as no new data was generated or analyzed in this study.

References

1. Hao, C.; Xu, L.; Kuang, H.; Xu, C. *Adv. Mater. (Weinheim, Ger.)* **2020,** *32,* 1802075. doi:10.1002/adma.201802075
2. Zhao, B.; Yang, S.; Deng, J.; Pan, K. *Adv. Sci.* **2021,** *8,* 2003681. doi:10.1002/advs.202003681
3. Niu, X.; Zhao, R.; Yan, S.; Pang, Z.; Li, H.; Yang, X.; Wang, K. *Small* **2023,** *19,* 2303059. doi:10.1002/smll.202303059
4. Chen, W.; Li, B.; Gao, G.; Sun, T. *Interdiscip. Mater.* **2023,** *2,* 689–713. doi:10.1002/idm2.12117
5. Satapathy, S.; Kumar, S.; Kurmi, B. D.; Gupta, G. D.; Patel, P. *Chirality* **2024,** *36,* e23698. doi:10.1002/chir.23698
6. Yasukawa, T.; Kuremoto, T.; Miyamura, H.; Kobayashi, S. *Org. Lett.* **2016,** *18,* 2716–2718. doi:10.1021/acs.orglett.6b01172
7. Lin, L.; Fukagawa, S.; Sekine, D.; Tomita, E.; Yoshino, T.; Matsunaga, S. *Angew. Chem., Int. Ed.* **2018,** *57,* 12048–12052. doi:10.1002/anie.201807610
8. Ye, C.-X.; Chen, S.; Han, F.; Xie, X.; Ivlev, S.; Houk, K. N.; Meggers, E. *Angew. Chem., Int. Ed.* **2020,** *59,* 13552–13556. doi:10.1002/anie.202004799
9. Yasukawa, T.; Miyamura, H.; Kobayashi, S. *Acc. Chem. Res.* **2020,** *53,* 2950–2963. doi:10.1021/acs.accounts.0c00587
10. Dey, P.; Rai, P.; Maji, B. *ACS Org. Inorg. Au* **2022,** *2,* 99–125. doi:10.1021/acsorginorgau.1c00032
11. Ankudinov, N. M.; Nelyubina, Y. V.; Perekalin, D. S. *Chem. – Eur. J.* **2022,** *28,* e202200195. doi:10.1002/chem.202200745
12. Mukherjee, N.; Mondal, B.; Saha, T. N.; Maity, R. *Appl. Organomet. Chem.* **2024,** *38,* e6794. doi:10.1002/aoc.6794
13. Zhang, S.-X.; Long, L.; Li, Z.; He, Y.-M.; Li, S.; Chen, H.; Hao, W.; Fan, Q.-H. *J. Am. Chem. Soc.* **2025,** *147,* 5197–5211. doi:10.1021/jacs.4c15673
14. Huang, K.-X.; Xie, M.-S.; Zhao, G.-F.; Qu, G.-R.; Guo, H.-M. *Adv. Synth. Catal.* **2016,** *358,* 3627–3632. doi:10.1002/adsc.201600377
15. Li, W.; Wiesenfeldt, M. P.; Glorius, F. *J. Am. Chem. Soc.* **2017,** *139,* 2585–2588. doi:10.1021/jacs.6b13124
16. Zhang, B.; Liu, L.; Guo, D.; Wang, J. *ChemistrySelect* **2019,** *4,* 1195–1198. doi:10.1002/slct.201803246
17. Zhou, Z.; Chen, S.; Hong, Y.; Winterling, E.; Tan, Y.; Hemming, M.; Harms, K.; Houk, K. N.; Meggers, E. *J. Am. Chem. Soc.* **2019,** *141,* 19048–19057. doi:10.1021/jacs.9b09301
18. van Leest, N. P.; van Vliet, K. M.; de Bruin, B. *Chem* **2020,** *6,* 1851–1853. doi:10.1016/j.chempr.2020.07.005
19. Miyazawa, T.; Suzuki, T.; Kumagai, Y.; Takizawa, K.; Kikuchi, T.; Kato, S.; Onoda, A.; Hayashi, T.; Kamei, Y.; Kamiyama, F.; Anada, M.; Kojima, M.; Yoshino, T.; Matsunaga, S. *Nat. Catal.* **2020,** *3,* 851–858. doi:10.1038/s41929-020-00513-w
20. Ye, C.-X.; Meggers, E. *Acc. Chem. Res.* **2023,** *56,* 1128–1141. doi:10.1021/acs.accounts.3c00081
21. Chen, L.-A.; Xu, W.; Huang, B.; Ma, J.; Wang, L.; Xi, J.; Harms, K.; Gong, L.; Meggers, E. *J. Am. Chem. Soc.* **2013,** *135,* 10598–10601. doi:10.1021/ja403777k
22. Huo, H.; Fu, C.; Harms, K.; Meggers, E. *J. Am. Chem. Soc.* **2014,** *136,* 2990–2993. doi:10.1021/ja4132505
23. Tan, X.; Zeng, W.; Wen, J.; Zhang, X. *Org. Lett.* **2020,** *22,* 7230–7233. doi:10.1021/acs.orglett.0c02565
24. Sheldon, R. A. *Green Chem.* **2016,** *18,* 3180–3183. doi:10.1039/c6gc90040b
25. Kumar, N.; Gastelu, G.; Zábranský, M.; Kukla, J.; Uranga, J. G.; Hulla, M. *Chem. Sci.* **2024,** *15,* 20573–20581. doi:10.1039/d4sc03665d
26. Bismuto, A.; Cowley, M. J.; Thomas, S. P. *ACS Catal.* **2018,** *8,* 2001–2005. doi:10.1021/acscatal.7b04279
27. Kobayashi, K.; Komatsuzaki, S.; Onozawa, S.-y.; Masuda, K.; Kobayashi, S. *Org. Biomol. Chem.* **2023,** *21,* 8259–8262. doi:10.1039/d3ob01266b
28. Hicks, J.; Vasko, P.; Goicoechea, J. M.; Aldridge, S. *Angew. Chem., Int. Ed.* **2021,** *60,* 1702–1713. doi:10.1002/anie.202007530
29. Gesslbauer, S.; Savela, R.; Chen, Y.; White, A. J. P.; Romain, C. *ACS Catal.* **2019,** *9,* 7912–7920. doi:10.1021/acscatal.9b00875
30. De, S.; Dutta, S.; Koley, D. *Organometallics* **2022,** *41,* 2132–2145. doi:10.1021/acs.organomet.2c00242
31. da Silva, E. M.; Vidal, H. D. A.; Januário, M. A. P.; Corrêa, A. G. *Molecules* **2022,** *28,* 12. doi:10.3390/molecules28010012
32. Gao, J.; Wang, P.; Shen, A.; Yang, X.; Cen, S.; Zhang, Z. *ACS Catal.* **2024,** *14,* 5621–5629. doi:10.1021/acscatal.4c00726
33. Wu, Y.; Zhu, C. *Chem. Commun.* **2025,** *61,* 5228–5233. doi:10.1039/d5cc01026h
34. Chitchak, K.; Jaisabuy, K.; Vanalabhpatana, P. *Catal. Lett.* **2025,** *155,* 173. doi:10.1007/s10562-025-04996-9
35. Lee, C. L.; Chen, D.; Chang, X.-Y.; Tang, Z.; Che, C.-M. *Organometallics* **2020,** *39,* 2642–2652. doi:10.1021/acs.organomet.0c00268
36. Bian, S.; Abbina, S.; Lu, Z.; Kolodka, E.; Du, G. *Organometallics* **2014,** *33,* 2489–2495. doi:10.1021/om401226j
37. Ni, C.; Ma, X.; Yang, Z.; Roesky, H. W. *Eur. J. Inorg. Chem.* **2022,** *2022,* e202100929. doi:10.1002/ejic.202100929
38. Zhong, M.; Yuan, M. *RSC Adv.* **2025,** *15,* 15052–15085. doi:10.1039/d5ra02549d
39. Keck, G. E.; Krishnamurthy, D.; Chen, X. *Tetrahedron Lett.* **1994,** *35,* 8323–8324. doi:10.1016/s0040-4039(00)74397-8
40. Bedeschi, P.; Casolan, S.; Costa, A. L.; Tagliavini, E.; Umani-Ronchi, A. *Tetrahedron Lett.* **1995,** *36,* 7897–7900. doi:10.1016/0040-4039(95)01627-t
41. Zhu, S. S.; Cefalo, D. R.; La, D. S.; Jamieson, J. Y.; Davis, W. M.; Hoveyda, A. H.; Schrock, R. R. *J. Am. Chem. Soc.* **1999,** *121,* 8251–8259. doi:10.1021/ja991432g
42. Chen, Y.; Yekta, S.; Yudin, A. K. *Chem. Rev.* **2003,** *103,* 3155–3212. doi:10.1021/cr020025b
43. Simonsen, K. B.; Svenstrup, N.; Roberson, M.; Jørgensen, K. A. *Chem. – Eur. J.* **2000,** *6,* 123–128. doi:10.1002/(sici)1521-3765(20000103)6:1<123::aid-chem123>3.0.co;2-l
44. Campbell, E. J.; Zhou, H.; Nguyen, S. T. *Angew. Chem., Int. Ed.* **2002,** *41,* 1020–1022. doi:10.1002/1521-3773(20020315)41:6<1020::aid-anie1020>3.0.co;2-s

45. Graves, C. R.; Zhou, H.; Stern, C. L.; Nguyen, S. T. *J. Org. Chem.* **2007,** *72,* 9121–9133. doi:10.1021/jo070563u
46. Adate, P. A.; Matsunaga, T.; Shin, H.; Harada, T. *Adv. Synth. Catal.* **2016,** *358,* 3688–3693. doi:10.1002/adsc.201600594
47. Li, Z.; Chen, P.; Ni, Z.; Gao, L.; Zhao, Y.; Wang, R.; Zhu, C.; Wang, G.; Li, S. *Nat. Commun.* **2025,** *16,* 735. doi:10.1038/s41467-025-56000-y
48. Pu, L. *Chem. Rev.* **2024,** *124,* 6643–6689. doi:10.1021/acs.chemrev.4c00132
49. Shibasaki, M.; Matsunaga, S. *Chem. Soc. Rev.* **2006,** *35,* 269–279. doi:10.1039/b506346a
50. Lin, Y.-M.; Fu, I.-P.; Uang, B.-J. *Tetrahedron: Asymmetry* **2001,** *12,* 3217–3221. doi:10.1016/s0957-4166(02)00008-3
51. Lebedev, Y.; Polishchuk, I.; Maity, B.; Dinis Veloso Guerreiro, M.; Cavallo, L.; Rueping, M. *J. Am. Chem. Soc.* **2019,** *141,* 19415–19423. doi:10.1021/jacs.9b10364
52. Zheng, L.; Yin, X.; Mohammadlou, A.; Sullivan, R. P.; Guan, Y.; Staples, R.; Wulff, W. D. *ACS Catal.* **2020,** *10,* 7188–7194. doi:10.1021/acscatal.0c01734
53. Kuroda, Y.; Park, K.; Shimazaki, Y.; Zhong, R. L.; Sakaki, S.; Nakao, Y. *Angew. Chem., Int. Ed.* **2023,** *62,* e202300704. doi:10.1002/anie.202300704
54. Shimazaki, Y.; Osawa, A.; Nakao, Y. *Asian J. Org. Chem.* **2024,** *13,* e202300487. doi:10.1002/ajoc.202300487
55. Tong, Y.; Liu, B.; Wu, Y.; Yang, B.; Wen, G.; Yang, Y.-T.; Chai, J.; Hu, X. *Sens. Actuators, B* **2017,** *252,* 794–802. doi:10.1016/j.snb.2017.04.161
56. Shaw, S.; White, J. D. *Chem. Rev.* **2019,** *119,* 9381–9426. doi:10.1021/acs.chemrev.9b00074
57. Matsumoto, K.; Saito, B.; Katsuki, T. *Chem. Commun.* **2007,** 3619–3627. doi:10.1039/b701431g
58. Ward, C. V.; Jiang, M.; Kee, T. P. *Tetrahedron Lett.* **2000,** *41,* 6181–6184. doi:10.1016/s0040-4039(00)01002-9
59. Jakhar, A.; Sadhukhan, A.; Khan, N. U.; Saravanan, S.; Kureshy, R. I.; Abdi, S. H. R.; Bajaj, H. C. *ChemCatChem* **2014,** *6,* 2656–2661. doi:10.1002/cctc.201402373
60. Breteler, M. R. T.; Zhong, Z.; Dijkstra, P. J.; Palmans, A. R. A.; Peeters, J.; Feijen, J. *J. Polym. Sci., Part A: Polym. Chem.* **2006,** *45,* 429–436. doi:10.1002/pola.21841
61. Gao, B.; Li, D.; Li, Y.; Duan, Q.; Duan, R.; Pang, X. *New J. Chem.* **2015,** *39,* 4670–4675. doi:10.1039/c5nj00469a
62. Evans, D. A.; Janey, J. M.; Magomedov, N.; Tedrow, J. S. *Angew. Chem., Int. Ed.* **2001,** *40,* 1884–1888. doi:10.1002/1521-3773(20010518)40:10<1884::aid-anie1884>3.0.co;2-9
63. Cozzi, P. G. *Chem. Soc. Rev.* **2004,** *33,* 410–421. doi:10.1039/b307853c
64. Baleizão, C.; Garcia, H. *Chem. Rev.* **2006,** *106,* 3987–4043. doi:10.1021/cr050973n
65. Bouyahyi, M.; Grunova, E.; Marquet, N.; Kirillov, E.; Thomas, C. M.; Roisnel, T.; Carpentier, J. F. *Organometallics* **2008,** *27,* 5815–5825. doi:10.1021/om800651z
66. Madhavan, N.; Weck, M. *Adv. Synth. Catal.* **2008,** *350,* 419–425. doi:10.1002/adsc.200700491
67. Guo, X.; Ahmed, H.; Xu, G.; Wang, Q. *Angew. Chem., Int. Ed.* **2025,** *64,* e202417075. doi:10.1002/anie.202417075
68. Ryu, H. K.; Cha, J.; Yu, N.; Lee, E.; Son, K.-s. *Inorg. Chem. Commun.* **2020,** *122,* 108278. doi:10.1016/j.inoche.2020.108278
69. Pada Majhi, T.; Teat, S. J.; Kundu, N. *J. Indian Chem. Soc.* **2022,** *99,* 100401. doi:10.1016/j.jics.2022.100401
70. Joo, J. M.; Kang, E. *Synthesis* **2023,** *56,* 1549–1562. doi:10.1055/s-0043-1763620
71. Damera, T.; Naga Gayatri, S.; Pagadala, R.; Abbu, V.; Palle, K.; Gullapelli, K. *ChemistrySelect* **2024,** *9,* e202402148. doi:10.1002/slct.202402148
72. Zhao, G.; Wang, K.; Qi, B.; Zhang, T.; Gong, Z.; Wang, Y.; Zhong, L.; Zheng, F. *Inorg. Chem.* **2026,** *65,* 6735–6743. doi:10.1021/acs.inorgchem.6c00008
73. Liu, J.; Ma, H. *Dalton Trans.* **2014,** *43,* 9098–9110. doi:10.1039/c4dt00353e
74. Dissanayake, D.; Forsyth, C.; Vidović, D. *Dalton Trans.* **2023,** *52,* 4063–4076. doi:10.1039/d3dt00206c
75. Ferreira, H.; Conradie, M. M.; Conradie, J. *Data Brief* **2019,** *22,* 436–445. doi:10.1016/j.dib.2018.12.043
76. Toda, H.; Kanega, R.; Yano, T.; Yoshikawa, T.; Kuriyama, S.; Himeda, Y.; Sakata, K.; Nishibayashi, Y. *Chem. Lett.* **2024,** *53,* upae040. doi:10.1093/chemle/upae040
77. Jia, B.; Hao, J.; Wei, X.; Tong, H.; Zhou, M.; Liu, D. *J. Organomet. Chem.* **2016,** *831,* 11–17. doi:10.1016/j.jorganchem.2016.12.031
78. Martínez, J.; Castro-Osma, J. A.; AlonsoMoreno, C.; RodríguezDiéguez, A.; North, M.; Otero, A.; LaraSánchez, A. *ChemSusChem* **2016,** *10,* 1175–1185. doi:10.1002/cssc.201601370
79. Hador, R.; Botta, A.; Venditto, V.; Lipstman, S.; Goldberg, I.; Kol, M. *Angew. Chem., Int. Ed.* **2019,** *58,* 14679–14685. doi:10.1002/anie.201906848
80. Hador, R.; Lipstman, S.; Rescigno, R.; Venditto, V.; Kol, M. *Chem. Commun.* **2020,** *56,* 13528–13531. doi:10.1039/d0cc05957a
81. Node, M.; Nishide, K.; Shigeta, Y.; Shiraki, H.; Obata, K. *J. Am. Chem. Soc.* **2000,** *122,* 1927–1936. doi:10.1021/ja993546y
82. Corminboeuf, O.; Renaud, P. *Org. Lett.* **2002,** *4,* 1735–1738. doi:10.1021/ol0257981
83. Itoh, H.; Maeda, H.; Yamada, S.; Hori, Y.; Mino, T.; Sakamoto, M. *Org. Chem. Front.* **2014,** *1,* 1107–1115. doi:10.1039/c4qo00222a
84. Ooi, T.; Saito, A.; Maruoka, K. *J. Am. Chem. Soc.* **2003,** *125,* 3220–3221. doi:10.1021/ja0292851
85. Nandi, P.; Solovyov, A.; Okrut, A.; Katz, A. *ACS Catal.* **2014,** *4,* 2492–2495. doi:10.1021/cs5001976

License and Terms

This is an open access article licensed under the terms of the Beilstein-Institut Open Access License Agreement (https://www.beilstein-journals.org/bjoc/terms), which is identical to the Creative Commons Attribution 4.0 International License (https://creativecommons.org/licenses/by/4.0). The reuse of material under this license requires that the author(s), source and license are credited. Third-party material in this article could be subject to other licenses (typically indicated in the credit line), and in this case, users are required to obtain permission from the license holder to reuse the material.

The definitive version of this article is the electronic one which can be found at:
https://doi.org/10.3762/bjoc.22.130